CHALMERS
UNIVERSITY OF TECHNOLOGY

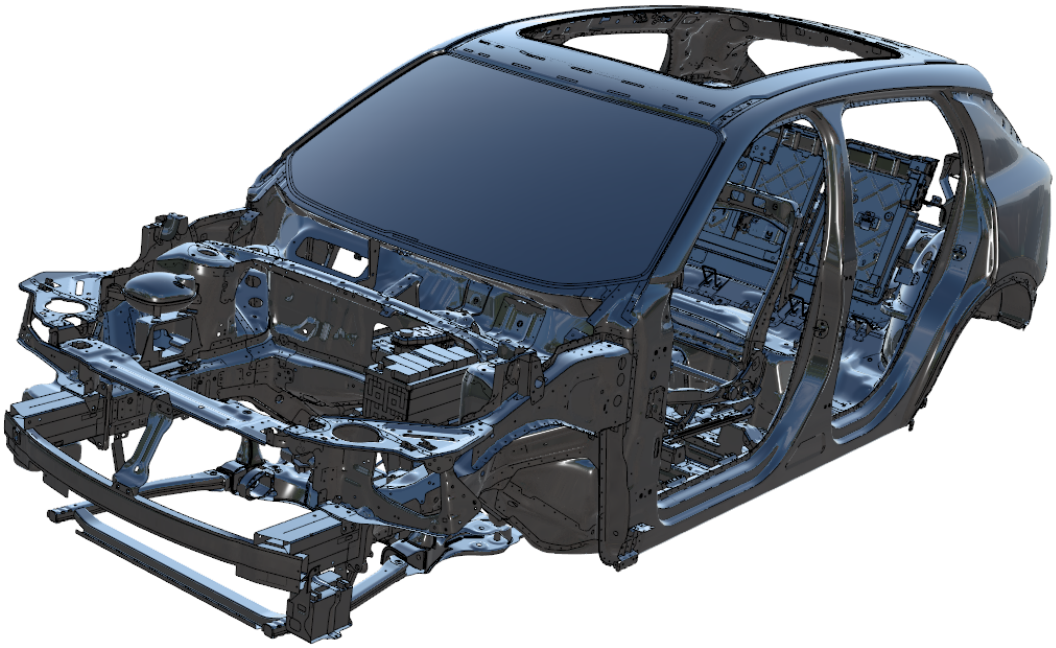

Deformations in Body Openings

Correlation between Vehicle Testing and Simulation Data

Master's thesis in Applied Mechanics

NERMA SARKIS KRIKOR
MOHAMED ZABEN

Department of Mechanics and Maritime Sciences
CHALMERS UNIVERSITY OF TECHNOLOGY
Gothenburg, Sweden 2019

Master's thesis 2019:06

Deformations in Body Openings

Correlation between Vehicle Testing and Simulation Data

NERMA SARKIS KRIKOR
MOHAMED ZABEN

CHALMERS
UNIVERSITY OF TECHNOLOGY

Department of Mechanics and Maritime Sciences
Division of Dynamics
Chalmers University of Technology
Gothenburg, Sweden 2019

Deformations in Body Openings
Correlation between Vehicle Testing and Simulation Data.
NERMA SARKIS KRIKOR
MOHAMED ZABEN

Examiner: Prof. Thomas Abrahamsson, Department of Mechanics and Maritime Science
Supervisor at company: Jens Weber

Master's Thesis 2019:06
Department of Mechanics and Maritime Science
Division of Dynamics
Chalmers University of Technology
SE-412 96 Gothenburg
Telephone +46 31 772 1000

Cover: Body in grey including windshield used in a body rig simulation.

Typeset in LaTeX
Gothenburg, Sweden 2019

Deformations in Body Openings
Correlation between Vehicle Testing and Simulation Data
NERMA SARKIS KRIKOR
MOHAMED ZABEN
Department of Mechanics and Maritime Science
Chalmers University of Technology

Abstract

A comprehensive complete vehicle test was performed within a thesis work by Alexander Jörud and Carl Jacobsson in order to measure the diagonal deformation in major body openings. Their main focus was on preparing and performing the physical test. They also updated the FE model to emulate the actual physical test. The aim with this thesis work is continue their study and to enable comparison between the simulation and test data. The correlation is performed in both time and frequency domains. The final aim is to identify the capability of the complete vehicle simulation procedure to predict body deformations.

A procedure to perform a correlation between simulation and physical test has been developed. This study is performed for three different road conditions: Belgian Pavé (PAV), Washboard in phase (WIP) and Washboard out of phase (WOP). The relative displacement is analysed for the car when driven at 30 km/h and 50 km/h on each road condition. The data is processed in order to perform the actual correlation study. This includes converting the data from acceleration to displacement and applying coordinate transformations. The E-line and Diagonal methods have been implemented in order to evaluate the distortion in all closure openings. This study consider time domain using the statistical evaluation (SEP) approach and also frequency domain analysis. For that reason three comparison filters have been developed.

An initial validation study resulted in a cutoff frequency at 5 Hz, as the accelerometers gave impercise data below these frequencies. Secondly, both rigid body and structural modes were identified between 5 and 20 Hz. Three different rigid body motions were clearly identified when analysing the local components of the E-line method. A modal analysis in the simulation code Adams was performed in order to analyse the different rigid body motions of the body, engine and wheel suspension further.

To prepare for correlation analysis the load level was compared between the physical test data measured using a wheel force transducer (WFT) and simulation data obtained with a Ftire model. Furthermore, the correlation study included a number of different criteria like influence from velocity, modal damping and road profile. The local and global component correlation pattern were analysed.

A clear pattern was identified for all load cases during the correlation investigation. For instance, the rear door was subjected to larger deformations than the front door. This pattern was present for all load cases. A likely explanation is that the structure of the car is stiffer close to the A-pillar, which is a closed section, compared to the open sections at the B and C pillars. Furthermore, the PAV road condition contributed to the highest displacement at all closure openings. Both PAV and WOP give torsional loads, causing a higher distortion at the sunroof and the tailgate compared to the side doors. A clear symmetry between left and right side of the vehicle was observed when evaluating the distortion in the side door openings. This was

also observed for the left and right side of the tailgate opening.

The absolute distortion value was compared between physical test and two simulations: one with 2% and one with 15% modal damping. The correlation between physical test and simulation varies clearly for the different openings. It was not possible to find one modal damping value to give a good correlation for all closure openings. Therefore, a deeper analysis is required to understand why certain modes give strong or weak contribution. However, when assessing all openings for all load cases it could be concluded that simulation with 2% modal damping is clearly over-predicting the relative motion, whereas simulation with 15% modal damping is slightly under-predicting as compared to the physical test. Finally the local component pattern was studied. For PAV only the front doors and the tailgate presented a clear pattern for physical test and simulation. The results for WOP solely presented a pattern for the tailgate opening. For WIP no clear no clear pattern was identified for any of the openings.

Keywords: Body opening distortion, correlation, modal analysis, E-line method, Adams, Diagonal method, modal damping

Acknowledgements

This master thesis project was conducted during spring 2019 at China Euro Vehicle Technology AB (CEVT) located at Lindholmen in Gothenburg. The participants in this thesis are students of Master of Science in Applied Mechanics with a bachelor degree in Mechanical Engineering.

We would like to thank our supervisor Jens Weber for supporting the group through all phases of the project. Jens has been an asset to the group with his expertise in computer aided engineering (CAE), ideas, feedback, time and encouragement. We would further like to thank Yassine Wardi for being an asset with his expertise in programming. We would also like to thank our examiner, Prof. Thomas Abrahamsson for his assistance.

Finally, we would like to thank Mikkel Grymer, Michael Léven, Joel Hultman, Yassine Wardi, Martin Ljunggren, Oskar Jonson, Markus Fritzell, Peter Appelgren and Lars Hansson for supporting the project through all phases.

Nomenclature

A-pillar	Structure at the front edge of the front door and wheel fender
B-pillar	Structure in-between front and rear door
BIG	Body in grey
C-pillar	Structure between the rear side windows and the rear window
CAE	Computer Aided Engineering
CCB	Cross Car Beam
CEVT	China Euro Vehicle Techonology
csv	Comma-separated values
FFT	Fast Fourier Transform
iFFT	Inverse Fast Fourier Transform
PAV	Belgian Pavé
pch	Punch
RBM	Rigid body motions
RMS	Root Mean Square
SEP	Statistical Evaluation Parameter
VCC	Volvo car corporation
WFT	Wheel force transducer
WIP	Washboard in phase
WOP	Washboard out of phase

Contents

List of Figures

List of Tables

1
Introduction

All components of the vehicle are excited due to the road load vibrations at different frequencies. This excitation causes relative movement between the interior parts, which can cause Squeak & Rattle (S&R) issues. The distribution of body stiffness affects how the body deforms under given loads. Minimizing S&R are of paramount importance when designing vehicles, as it enhances the perceived quality of the vehicle. Traditionally, S&R issues are often detected late in the developing stage, using instruments placed on a complete assembled vehicle. Unfortunately, correcting errors at this late stage is both expensive and time consuming. Thus, S&R issues may best be detected early by studying the deformation of the vehicle body with the help of simulations. The diagonal relative displacement, see Figure 2.6, was measured as the body closure openings captures the complexity of the overall body stiffness. This enables engineers to predict S&R issues at early stage. It is essential to ensure that the simulations are representative. This is done by comparing the results obtained from conducted simulation with physical tests.

During spring 2018, Alexander Jörud and Carl Jacobsson performed a master thesis on behalf of CEVT. The aim of their work was to establish a test and simulation procedure, which enables comparison between the tested and simulated relative displacement in all closure body openings for a car driving on varying test tracks at different velocities. The physical test was performed at Volvo Car Corporation at Torslanda and Hällered Proving Grounds. The acceleration was measured in predefined locations of the body and the upper area of the instrument panel. The available physical test data was then used for correlation work with a complete vehicle simulation model.

The complete vehicle simulation was developed with focus on durability. The scanned road profiles were used in simulation with Adams in order to obtain reliable and realistic results. This simulation process has found increased use for the solidity attribute. As a result, new requirements were developed for both exterior and interior components of the car. These new requirements includes evaluation of the relative displacement in predefined locations, e.g. in all closure openings of the body or in different zones of an instrument panel.

Jacobsson and Jöruds master thesis presented the diagonal displacement in all body closure openings based on complete vehicle testing of the Lynk & Co 01. The main aim of their work was to conduct the pre-processing part for both test and simulation. Their results became the base for this work. The main aim here is to

compare the physical test data with the simulated data. An important task is to identify the simulation parameters, which can improve the correlation with the test data. In order to perform this correlation a wide range of different aspects have been considered:

- Understanding the CAE representation of a complete vehicle.
- The theory of modal transient analysis.
- Efficient handling of test data by creating Python scripts.
- Test specific aspects like rigid body modes, converting acceleration to displacement.
- Comparison of the diagonal method with the E-line method.
- Time and frequency domain correlation.

2
Modelling and Test Aspects

This section briefly describes the theory behind the structure of the car body, test and simulation aspects and the procedure behind the data processing.

2.1 Car body

Three important parts of the car body is the A, B and C-pillar. The pillars purpose is to offer substantial support for window areas and roof of the car. The A-pillar is located between the front edge of the front door and wheel fender. It provides the windshield with support, whereas the B-pillar is placed in-between the front and rear door. It is welded to the roof, rock panel and floor panel [1]. The purpose with the B-pillar, also called centre pillar, is to support the roof panel. Lastly, the C-pillar is located next to the rear door and back fender. As a result, the C-pillar provides substantial support for the tailgate openings.

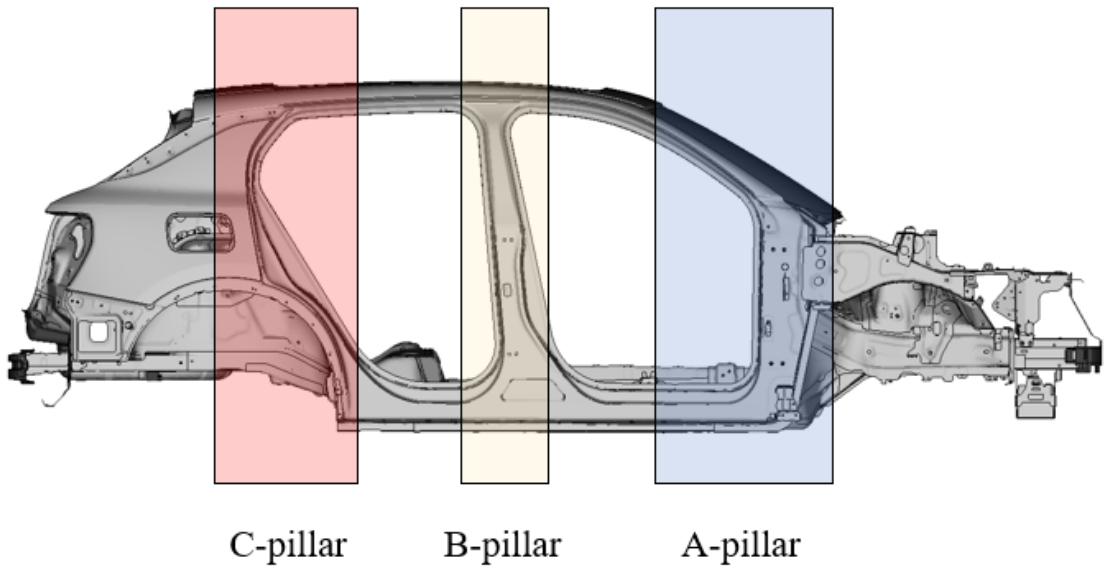

Figure 2.1: A, B and C-pillars on the car body

2.2 Physical test

The physical test was conducted driving the Lynk & Co. 01 car under well defined conditions on varying tracks with different velocities. The purpose was to measure the deformation in all closure openings of the vehicle.

The actual physical test phase was conducted on 23 of May 2018 by Jacobsson and Jörud [2]. The provided car was manufactured 2016 and had a total weight of 1710 kg in the absence of luggage, passengers and driver. Summer tires were mounted on the car prior the actual physical test. A WFT was installed on the right front wheel in order to measure the loads affecting the vehicle [2].

Furthermore, the actual physical test was conducted by a test driver from Volvo Car Corporation (VCC) at Hällered proving ground. The test driver drove several laps on WOP, WIP and PAV at constant speed [2]. These tracks are explained further in Section 2.5.

2.2.1 Physical test equipment

The physical test equipment consists of 12 accelerometers and one WFT placed on right front wheel. The equipments are described in detail below.

2.2.1.1 Accelerometers

During the physical test, integrated circuit piezo electric accelerometers were applied on the physical car. One of the used accelerometers is shown in Figure 2.2. Piezoelectric sensors can be used to measure pressure, acceleration or force. The sensors used here measures the acceleration in three orthogonal direction.

The mechanism behind the piezoelectric sensor is based on solid materials that deform due to applied 3D stress state. As a result, electric charges proportional to the applied stress is generated. Furthermore, calibration factors are given for each accelerometer. There calibration factors, together with the generated electric charge, enables the recording of acceleration. Additionally, the accelerometers are able to accurately measure acceleration at frequencies above 2 Hz according to the manual [3],[4].

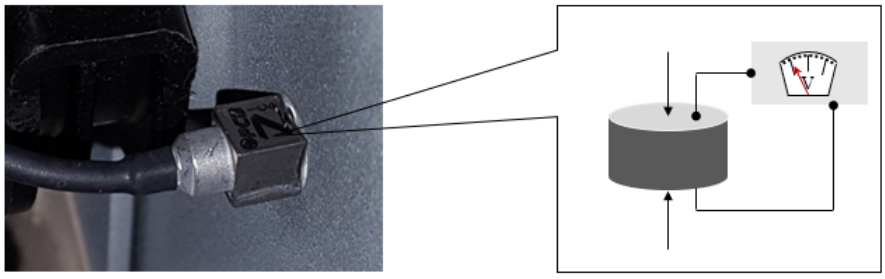

Figure 2.2: Accelerometer with a piezoelectric sensor inside.

Furthermore, the three major axis of the accelerometers are aligned with the global coordinate system. A total of six accelerometers where placed on the front and rear doors, four on the tailgate and two on the sunroof. See Figure 2.3 for some position of the accelerometers.

However, the two accelerometers placed on the sunroof could not be aligned properly due to the natural curvature of the sunroof. As a result, adjustments where later conducted and implemented into the "coordination transformation" tool by Jacobsson and Jörud [2].

2.2.1.2 WFT

The forces and moments affecting the wheels can be measured using a WFT. A WFT consist of strain gauges and an electrical conductor connected to a film. The mechanism behind the strain gauge is determined by strain in the film. The change in the deformation of the film will result in a change in resistance and the strain can be determined from that. The strain gauges are attached to the wheel transducer and the signal from the strain gauge is used to calculate the spindle forces. The information regarding the deformation is then used to compute the forces affecting on the strain gauge [5],[6].

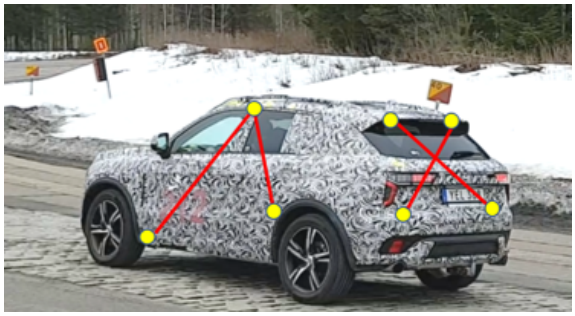

Figure 2.3: Position of the accelerometers on the physical car.

Figure 2.4: WTF placed on right front wheel

2.3 Data validation

It is importent to validate data when performing a correlation study. This phase of the project was conducted by a CEVT employee. The physical test data was validated by studying the relative displacement obtained from two accelerometers placed close to each other. One accelerometer was placed on the fender, while the other was placed on the hood. The results from the test is presented in Figure 2.5.

The lowest structural mode occur at 20 Hz and no relative motion is expected below 4 Hz. The only possible explanation is that the accelerometers are imprecise at frequencies below 4 Hz. Therefore, a filter with cut-on frequency at 5 Hz was introduced in order to ensure that non-valid data do not pollute the physical test data.

2.4 Complete vehicle simulations

The purpose of the complete vehicle simulations is to drive the studied vehicle on varying tracks with different velocities in order to measure the distortion in all closure openings of the vehicle. The studied openings are presented in Figure 2.6.

The complete vehicle simulation is conducted in MSC Nastran with help of a modal transient analysis. Additionally, the complete vehicle simulation is inflicted with external forces. The main purpose with these forces is to imitate physical forces during motion. The external forces where created by the Chassis & Powertrain Dynamic CAE group at CEVT in Adams.

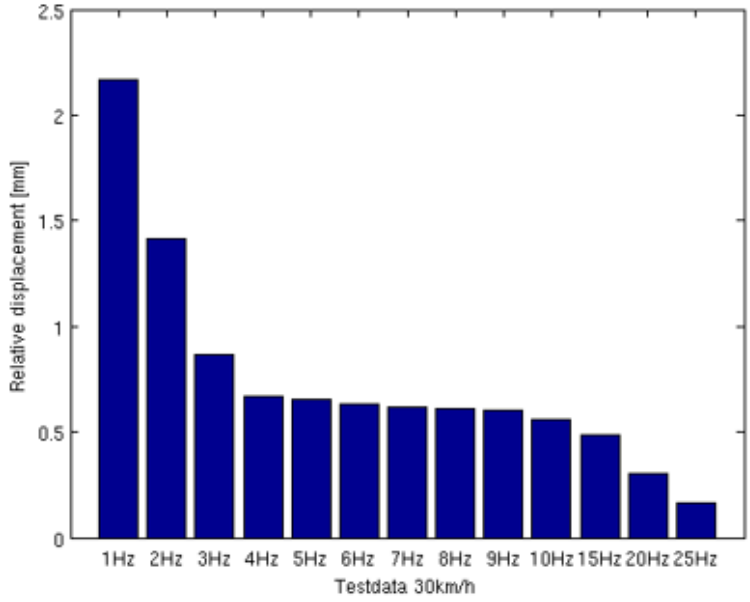

Figure 2.5: Cut-off filter on all closure openings of the car with SEP 30% value applied on Δy for physical test 30 km/h driving on PAV.

2.4.1 Vehicle used during simulation

The model used when performing the simulation is a FE model of the studied car. The FE model contains a trimmed body in grey (BIG). The BIG is the core structural of the vehicle, different views of the BIG is presented in Figure 2.6. Whereas the trim includes all parts attached to the body, such as the bumper and doors. The simulated vehicle model was adapted in order to resemble the physical vehicle.

2.4.2 Superelement

A complete vehicle simulation demands enormous computer capacity. This difficulty may be alleviated by reducing the amount of degrees of freedom with the help of superelements. Superelement can essentially be seen as representation of structural components, mainly used to represent non-crucial parts of a structure.

2.4.3 Software

The complete vehicle simulations was performed using a set of softwares. Among these is Adams. Adams is a multibody dynamic computer software used to study the motion of rigid and flexible components, including non-linear problems. The road conditions were scanned and put into Adams in order to ensure that the simulating environment is representative of the physical environment. Adams simulations produced data for 84 forces corresponding to data in a measurement channel. The obtained results were then used as input data to run a body rig simulation using the FE solver MSC Nastran. The model analysis in Adams is new to the Chassis & Powertrain Dynamic CAE group at CEVT and the application is still under method development.

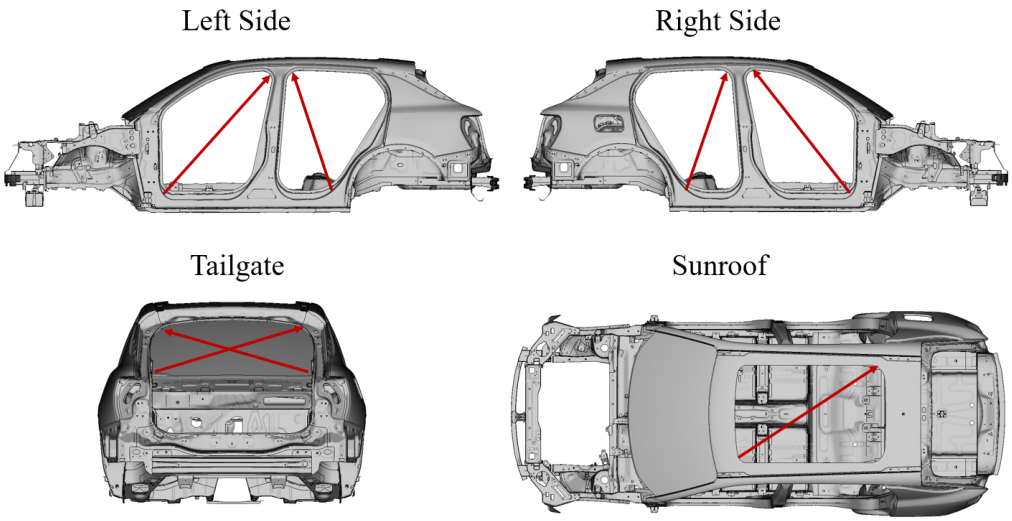

Figure 2.6: Diagonals of all closure openings marked on the studied vehicle from four different views.

Ansa is a pre-processing tool developed by BETA CAE. Ansa enables users to create a finite element model base on a CAD model [8]. The car was cut by the chassi and dynamic forces were applied underneath the car using the computer software Ansa. Meta is a multidisciplinary CAE post-processing software also developed by BETA CAE. It provides the user with python script editors. This editors enables automation and efficient data-processing [9].

2.4.4 Body rig simulation

The relative displacement can be computed on requested nodes using the body rig simulation tool, here MSC Nastran. It can be obtained either in local or global coordinate system, depending on the user request.

2.4.5 Virtual multi-stethoscope

The purpose with the virtual multi-stethoscope is to measure the deformation at all closure openings of the complete vehicle simulation. It is presented in Figure 2.7, where each node has a local coordinate system. The multi-stethoscope is placed on the car during the body rig simulation in order to specify where to measure the displacements. It was initially developed in Ansa by Jacobsson and Jörud [2].

The multi-stethoscope contains of 14 nodes, 7 master and 7 slave nodes. Each node pair has a unique local cartesian coordinate system defined by three nodes. These three nodes are presented in Table 2.1.

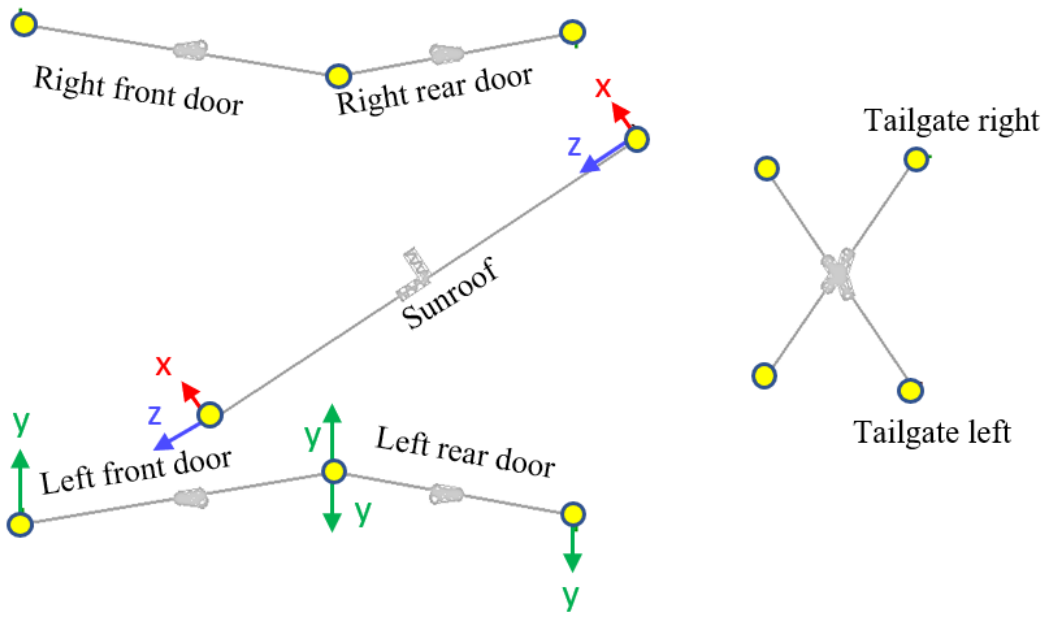

Figure 2.7: The top view of the multi-stetoscope with local coordinates present at each node.

Table 2.1: Local coordinate definition for each master node of the multi-stethoscope.

Closure opening	Node number	Coordinate system definition
Front door left	201001	201001 202001 207001
Rear door left	207001	207001 208001 201001
Front door right	209001	209001 210001 215001
Rear door right	215001	215001 216001 209001
Sunroof	219001	219001 220001 22
Tailgate left	221001	221001 222001 223001
Tailgate right	223001	223001 224001 221001

The local z coordinate is directed along the diagonal for the opening, pointing from the master to slave node. Local y coordinate is pointed normal to the outside of the car. Lastly, the x coordinate is normal to the diagonal in the opening plane. Each node is determined by a unique position and coordinate system. It's first digit indicates which coordinate system is used, where 1 and 2 stands for global respectively local coordinate system. The following five digits represent the position and indicates whether it is a master or slave node. The type of nodes is indicated by the second and third digit. The node is a slave node if the second and third digit combined give an even number and a master node if they combine to an odd number.

For instance, node 201001 is in local coordinate system. It is also a master node, since 01 is odd. The five last digits contains information about the closure opening, which in this case is 01001 for left front door. The different closure openings with corresponding coordinate system is presented in Table 2.1. Node 22 is introduced to correct for a sunroof coordinate system that is misaligned during the physical test.

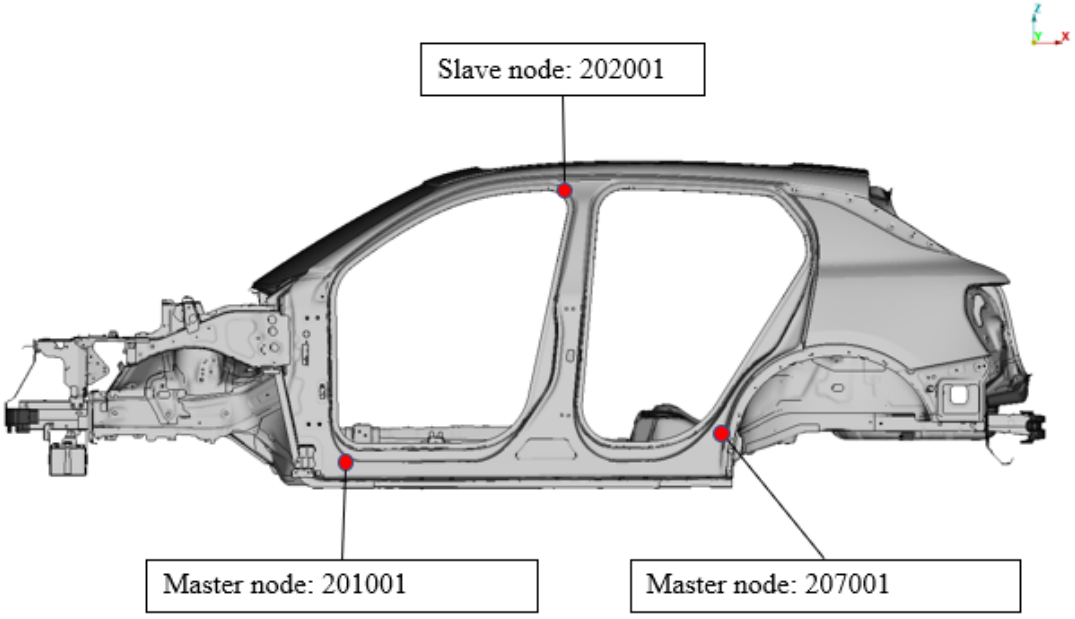

Figure 2.8: Coordination system definition of node number 201001

2.4.6 Modal analysis

The purpose with a modal analysis is to study the natural frequencies and mode shapes of a system governed by the differential equation. The natural eigenfrequencies is calculated using an equation stemming from the structural dynamics equation for enforced motion

$$\boldsymbol{M\ddot{u}}(t) + \boldsymbol{C\dot{u}}(t) + \boldsymbol{Ku}(t) = \boldsymbol{P}(t) \tag{2.1}$$

Here **M** is the mass matrix, **C** is the damping matrix, **K** is the stiffness matrix and **P** is the loading. The nodal displacement is denoted by **u**. Moreover, the nodal velocity and nodal acceleration $\ddot{\mathbf{u}}$ can be obtained by differentiating the nodal displacement once resptectiely twice with respect to time. The eigenvalues and eigenvectors can now be computed using the homogenous undamped part of equation (2.1) as follows

$$[\boldsymbol{K} - \boldsymbol{\omega^2 M}]\boldsymbol{\Phi} = 0 \tag{2.2}$$

where $\boldsymbol{\omega}^2$ are the eigenvalues and $\boldsymbol{\Phi}$ are the eigenvectors obtained as column vectors in matrix $\boldsymbol{\Phi}$.

2.4.7 Modal transient analysis

In order to study the response of a structure exposed to dynamic force a modal transient analysis is carried out. This method is efficient when computing the transient response of a structure exposed to excitation in time domain following the relation

$$\boldsymbol{\phi^T M \phi \ddot{\xi}} + \boldsymbol{\phi^T C \phi \dot{\xi}} + \boldsymbol{\phi^T K \phi \xi} = \boldsymbol{\phi^T P(t)} \tag{2.3}$$

As final step, the equation of motion is expressed using the orthogonality property in terms of generalised mass, damping and stiffness matrices defined as

$$\bar{\boldsymbol{M}} \triangleq diag(m_i) = \boldsymbol{\phi^T M \phi}, \quad \bar{\boldsymbol{C}} = \boldsymbol{\phi^T C \phi}, \quad \bar{\boldsymbol{K}} \triangleq diag(k_i) = \boldsymbol{\phi^T K \phi} \tag{2.4}$$

The matrices $\bar{M}$ and $\bar{K}$ are uncoupled since they do not contain off-diagonal terms that couples the equation of motion. Hence, the modal equations of motions are uncoupled in this form under some restriction for damping. Note that when modal damping is applied, each mode will have a damping c_i. The resulting decoupled equations of motion can be stated as

$$\ddot{\xi}_i(t) + 2c_i\omega_i\dot{\xi}_i(t) + \omega_i^2\xi_i(t) = \frac{1}{m_i}\phi_i^T P(t) \tag{2.5}$$

With $\omega_i^2 = k_i/m_i$ the response from a virgin state for each mode can now be derived using the following equation

$$\xi_i(t) = e^{\frac{c_i t}{2m_i}} \frac{1}{m_i\omega_i} \int_o^t e^{\frac{c_i \tau}{2m_i}} \phi_i^T P(\tau) sin\omega_i(t-\tau) d\tau \tag{2.6}$$

and superposition gives the displacements as

$$\boldsymbol{u}(t) = \boldsymbol{\phi}\boldsymbol{\xi}(t) \tag{2.7}$$

Modal damping is an efficient way to define a global damping as a function of the natural frequencies during the simulation. Each mode can be specified by a unique damping value, where each mode is damped independently of the remaining modes. The damping matrix $\bar{C}$ for a modal transient analysis follows as

$$\bar{C} = diag(c_i) \tag{2.8}$$

The modal damping coefficient c_i is defined as

$$c_i = g_i \omega_i m_i \tag{2.9}$$

where ω_i defines the undamped vibration frequency, g_i is the dimensionless damping coeffient and m_i is the mass defined as

$$m_i = \phi^T \boldsymbol{M} \phi \tag{2.10}$$

The modal damping impact will be analysed during the parameter study [10].

2.5 Test tracks

The roads presented below were used when performing both the physical test and simulation. The physical test, conducted on Hällered proving ground is illustrated in Figure 2.10. The CAD data of the road profile is used as input to the Ftire model used in Adams. The Ftire, see Figure 2.9, is a software module which represents the mechanical properties of the tire. The forces in the wheel axis can be calculated based on the interaction between the tire and the road.

WOP and WIP are periodically distributed between point a and b in Figure 2.10. The distance between each washboard wave decreases while the velocity of the vehicle is kept. This increases the frequency of the vibration caused by the road. Furthermore, the circular track is made of PAV. The VCC test driver drove at 30 km/h and 50 km/h over PAV in a clockwise direction on the track. The point c in Figure 2.10 is the starting position for the driver. The 30 km/h end position is located at point c" whereas the end position for the 50 km/h drive is located at c'. The different track lengths are specified to ensure equal duration for both PAV cases.

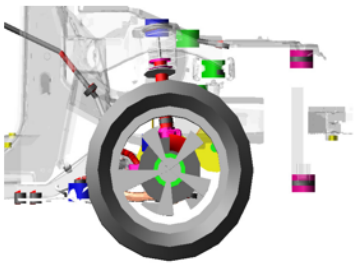

Figure 2.9: Illustrations of components used in the FTire model

The WOP track consists of-out-of phase bumps. This road condition causes the right hand side wheels to hit a bump, while the left wheels are ub the valleys between the bumps. As a result, the left and right wheels are moving out of phase with respect to each other. The road profile used in Adams is visualized in Figure 2.11.

The WIP track consists of aligned bumps, as seen in Figure 2.12, causing the front wheels on both sides of the car to hit the bumps simultaneously. As a result, the front wheels will move in-phase with respect to each other [11].

The PAV consists of randomly placed rectangular quarried stones as seen in fig 2.13.

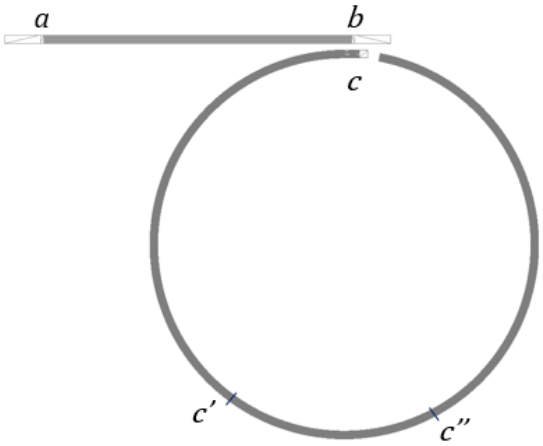

Figure 2.10: Top view of the tracks driven on at Hällered proving ground.

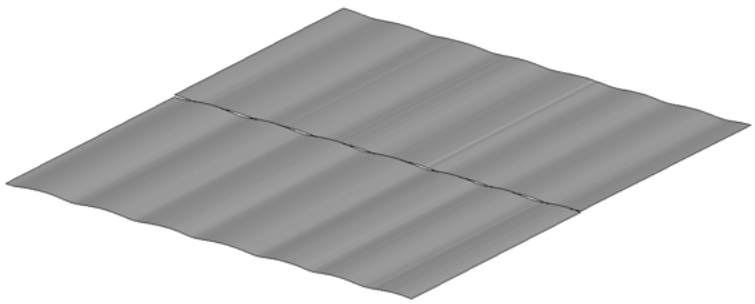

Figure 2.11: Adams model of WOP track.

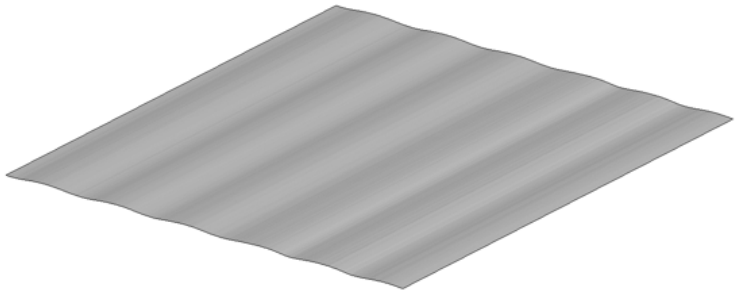

Figure 2.12: Adams model of WIP track.

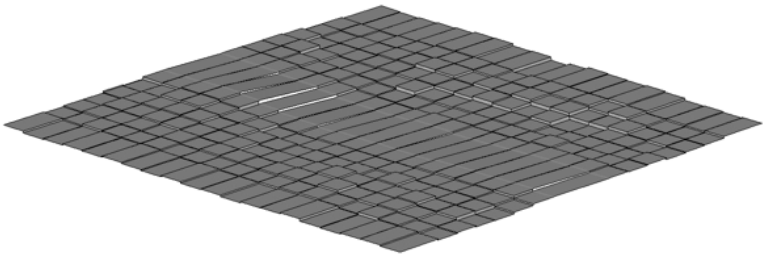

Figure 2.13: Simulated PAV road used in Adams

2.6 Data processing of physical test and simulation data

Data processing of physical test and simulation data is made to enable comparison. The physical test data contains information regarding the vehicle acceleration in all closure openings, while the simulation data contains displacement data. The physical test must therefore undergo transformation from acceleration to displacement in order to enable computation of the relative displacements.

The relative displacements are computed using two methods: The E-line and Diagonal methods. Both methods are applied on node pairs, where each node pair consist of master and one slave node. The E-line method evaluate the relative displacement in local coordinate direction, whereas the Diagonal method is evaluating the relative displacement based on global coordinate.

2.6.1 csv to pch format

Most of the scripts developed prior to following master thesis requires Nastran punch (pch) files as inputs. This causes issues since the raw acceleration data from VCC is given in comma separated values (cvs) format. The physical test data is therefore converted from csv to pch format. This is done using the python script "csv to pch" developed at CEVT.

2.6.2 Acceleration to displacement

The physical test data, which originally contains acceleration data, must be converted to displacement since the purpose is to study the displacement in all closure openings. The python script "acceleration to displacement" developed by CEVT is used to convert the data. The script is based upon Siemens LMS FAQ's Time domain integrating method [12].

The time domain integrating method is preceded by removing low frequencies by subtracting the time signal with a regression polynomial of order 6^{th} or lower. The time signal is thereafter re-sampled to 4000 Hz and integrated to velocity by numerical means. The integrated time signal is then filtered in order to remove linear trends. The integration and filtering of the processed time signal is repeated and the time signal is in that process re-sampled to 1000 Hz .

2.6.3 Time cut

The physical test contains several laps for each road case. A so-called "time selecting tool" is used to separate the laps and remove non-valid data. The simulation data is adapted to a sequence equal to the duration of the physical test data.

2.6.4 Coordination transformation

The transformation matrix, defined by rotational matrices $\mathbf{R_x}$, $\mathbf{R_y}$ and $\mathbf{R_z}$, is used to transform the relative displacement from global $[X,\ Y,\ Z]$ to local $[x,\ y,\ z]$ coordinates. The rotational matrices represents an anti-clockwise rotations θ_x, θ_y and θ_z for all directions according to the right hand rule. The rotational matrices are presented below.

$$\mathbf{R_x} = \begin{bmatrix} 1 & 0 & 0 \\ 0 & cos(\theta_x) & -sin(\theta_x) \\ 0 & sin(\theta_x) & cos(\theta_x) \end{bmatrix} \tag{2.11}$$

$$\mathbf{R_y} = \begin{bmatrix} cos(\theta_y) & 0 & sin(\theta_y) \\ 0 & 1 & 0 \\ -sin(\theta_x) & 0 & cos(\theta_x) \end{bmatrix} \tag{2.12}$$

$$\mathbf{R_z} = \begin{bmatrix} cos(\theta_z) & -sin(\theta_x) & 0 \\ sin(\theta_z) & cos(\theta_z) & 0 \\ 0 & 0 & 1 \end{bmatrix} \tag{2.13}$$

The transformation matrix is computed using equation 2.14 once the rotation matrices are obtained.

$$\mathbf{T} = \mathbf{R_x R_y R_z} \tag{2.14}$$

Equation (2.15) is used in order to transform the relative displacement from the global $\mathbf{X}$ to local $\mathbf{X'}$ coordinates [13].

$$\mathbf{XT} = \mathbf{X'} \tag{2.15}$$

Where

$$\mathbf{X} = \begin{bmatrix} x & y & z \end{bmatrix}^T \qquad \mathbf{X}' = \begin{bmatrix} X & Y & Z \end{bmatrix}^T \tag{2.16}$$

2.6.5 E-line method

The E-line method evaluates the relative displacement for each node in the local coordinate directions. The coordinate system for the node pairs is aligned with corresponding local coordinate system of the opening as seen in Figure 2.14. The local z coordinate is directed in diagonal direction of the closure opening.

The indexes m and s denotes master and slave, respectively. The E-line method allows to calculate three displacement values: Δx, Δy and Δz. The method is conducted by subtracting the local displacement value of the slave node from the master node according to equations (2.17)-(2.19).

$$\Delta x(t) = x_m(t) - x_s(t) \tag{2.17}$$
$$\Delta y(t) = y_m(t) - y_s(t) \tag{2.18}$$
$$\Delta z(t) = z_m(t) - z_s(t) \tag{2.19}$$

where $x(t)$, $y(t)$ and $z(t)$ are the displacements in corresponding direction at time t. The displacements for the master and slave node in local coordinate directions are illustrated in Figure 2.15.

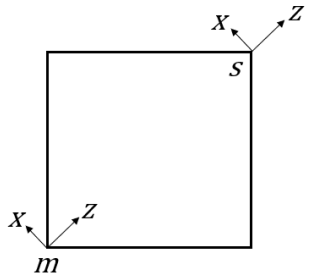

Figure 2.14: Undeformed two-dimensional geometry with local coordinates for both the master (m) and slave (s) node.

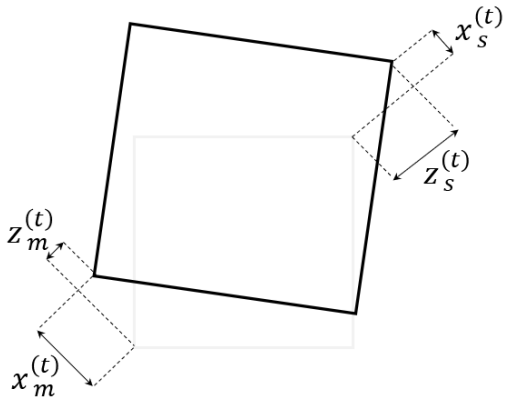

Figure 2.15: Displacement state for two-dimensional geometry for both master and slave node in local coordinate direction.

2.6.6 Diagonal method

The Diagonal method evaluates the relative diagonal displacement based on global displacement data. This method represent the structural deformation by a scalar closure metric. The master and slave nodes with corresponding initial distance and global coordinate system are illustrated in Figure 2.16. The deformed diagonal D_N illustrated in Figure 2.17 is initially computed according to equation (2.20).

$$D_N = \sqrt{(x_s(t) + x_0 - x_m(t))^2 + (y_s(t) + y_0 - y_m(t))^2 + (z_s(t) + z_0 - z_m(t))^2} \tag{2.20}$$

Where x, y and z are the displacements in global X, Y and Z direction. The index (0) denotes separations in the undeformed state. The undeformed diagonal D_0 illustrated in Figure 2.16 is subtracted from D_N in order to obtain the relative displacement in the diagonal direction.

$$\Delta D = D_N - D_0 \tag{2.21}$$

The displacements for the master and slave nodes in the global coordinate directions are illustrated in Figure 2.17.

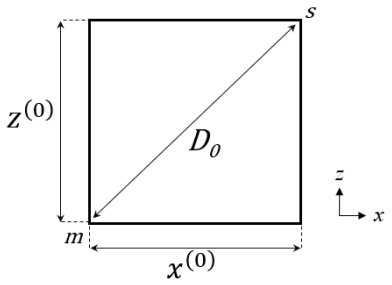

Figure 2.16: Undeformed two-dimensional geometry with initial distances between master and slave node.

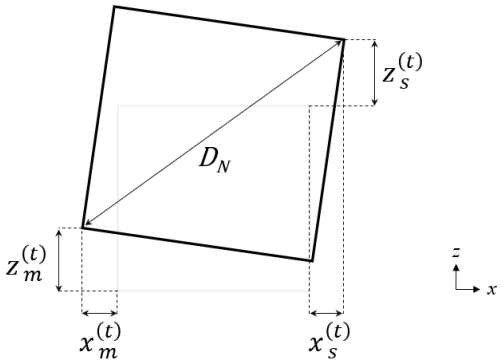

Figure 2.17: Deformed two-dimensional geometry, with displacement for both master and slave nodes in global coordinate direction

2.7 Identifying large displacements

It is possible to compare the relative displacements ΔD of the Diagonal method and Δz of the E-line method since both displacements describes the diagonal deformation between the node pairs. An extensive analysis of the relative displacements can lead to a better understanding of deformation behaviour during varying deformation angles. A simple way to demonstrate the displacement response is to apply it to two-dimensional structure, as shown in Figure 2.23. The master node, node a, is fixed in translation and rotation thus resulting in $\Delta z = \Delta z_s$. Furthermore, the left and right structure presents large and small deformations respectively. b is at the slave node in its undeformed nodal position, while B is in its deformed position.

In Figure 2.23 $\left|\overline{ab}\right| = \left|\overline{aB'}\right|$. The distance $\overline{B'B}$, which corresponds to ΔD, increases with increased α for square Δz according to Figure 2.18. Additionally, ΔD approaches Δz when α decreases toward zero. Hence, $\Delta D = \Delta z$ for small deformation and $\Delta D \neq \Delta z$ for large deformation. Thus, a comparison of E-line and Diagonal can be used to identify displacements due to large rotations caused by rigid body modes (RBM).

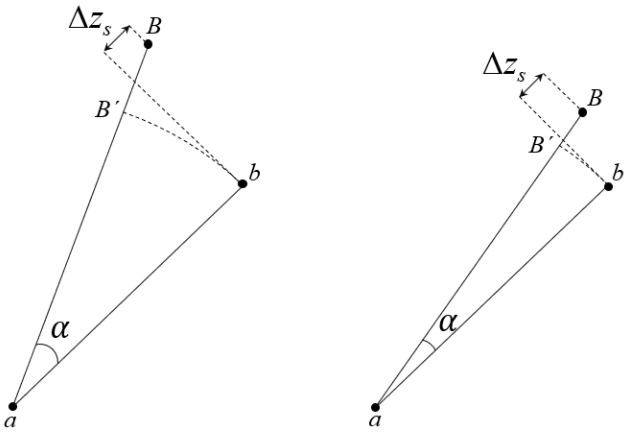

Figure 2.18: Deformed geometry metric Δzs according to Diagonal and E-line method

2.8 SEP

The SEP procedure is initiated by sorting the time signal from highest to lowest value. This is followed by calculating the mean value for a certain percentage of the highest values. The SEP is mainly used to represent the time history with one mean value.

2.9 Root mean square

The root mean square (RMS) procedure is an efficient way to represent the "strength" of a sequence which include both positive and negative values. The equation used to compute the RMS is [14]

$$x_{RMS} = \sqrt{\frac{x_1^2 + x_2^2 + ... + x_n^2}{n}} \tag{2.22}$$

2.10 Comparison filters

The displacement acquired from the experimental test and simulation are obtained as time domain data. However, the frequency domain counterpart makes it easier to study the mode contribution to the displacement. This is done by applying filters on the time data before computing the SEP value. The time signal data is filtered through cumulative, cut-off and bandpass filter as specified below.

Fast Fourier transform (FFT) is an algorithm mostly used to convert data from time to frequency domain. The inverse fast Fourier transform (iFFT) operation can be used to selective studies of a certain frequency range contributors to the time domain data. This operation is executed by applying a bandpass in a certain interval before the data is transformed back to time domain [15].

2.10.1 Cumulative

The cumulative filter is based upon accumulating frequencies as follows

$$\begin{aligned} f_c^{(1)} &= [n_c,\ n_c + 1]\ \text{[Hz]} \\ f_c^{(2)} &= [n_c,\ n_c + 2]\ \text{[Hz]} \\ &\vdots \\ f_c^{(n)} &= [n_c,\ n_{max}]\ \text{[Hz]} \end{aligned}$$

where n_{max} is the truncation frequency, n_c is the cut-on frequency and n is number of frequencies used for the cumulative filter. The derivative of the cumulative graph is used to identify the mode contribution.

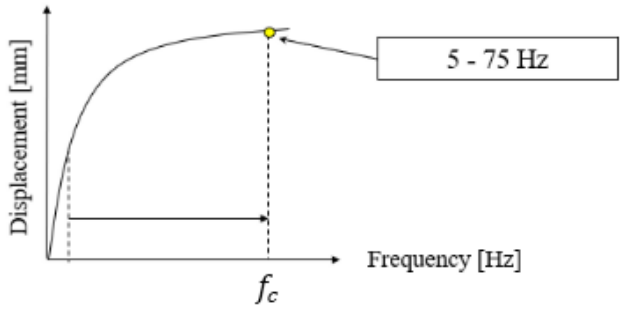

Figure 2.19: Cumulative filter for the frequency range between 5-75 Hz.

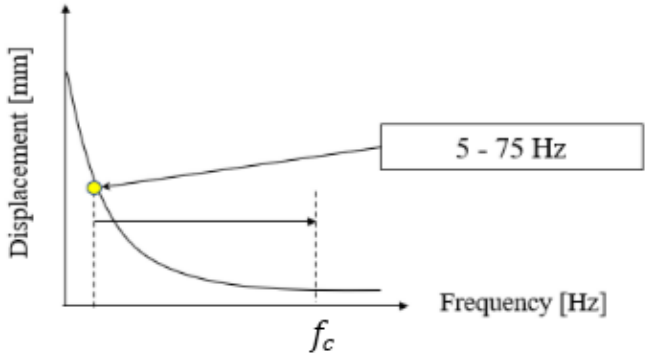

Figure 2.20: Cut-off filter for the frequency range between 5-75 Hz.

2.10.2 Cut-off

The cut-off procedure which is the inverse of the cumulative is conducted by decreasing the number of frequencies toward towards an upper frequency n_{max} as follows

$$
\begin{aligned}
f_{co}^{(1)} &= [n_c,\ n_{max}]\ \text{[Hz]} \\
f_{co}^{(2)} &= [n_c + 1,\ n_{max}]\ \text{[Hz]} \\
&\vdots \\
f_{co}^{(n)} &= [n_{max} - 1,\ n_{max}]\ \text{[Hz]}
\end{aligned}
$$

2.10.3 Bandpass

The purpose with bandpass filters is to isolate a very narrow frequency range as follows

$$
\begin{aligned}
f_b^{(1)} &= [n_c,\ n_c + 1] \ \text{[Hz]} \\
f_b^{(2)} &= [n_c + 1,\ n_c + 2] \ \text{[Hz]} \\
&\vdots \\
f_b^{(n)} &= [n_{max} - 1,\ n_{max}] \ \text{[Hz]}
\end{aligned}
$$

The bandpass filters is used to understand how varying frequencies affects the relative displacement. Furthermore, the bandpass filter is the positive and negative gradients of cut-off and cumulative filters respectively.

2.10.4 Spectral leakage

As stated by Fourier transformation theory, all signals can be described as summation of a unique set of sinusoidal waves. When the signal does not contain an integer number of periods over the time range due to transformation, so called spectral leakage occurs. As a result, it causes frequency and amplitude errors of the frequency spectrum.

Spectral leakage may be identified by comparing original data to that of forward and inverse transformation. An example of showing the effect of leakage is given in Figure 2.22. The data is assumed to be free from spectral leakage if the original data is identical to the data of inverse Fourier transform.

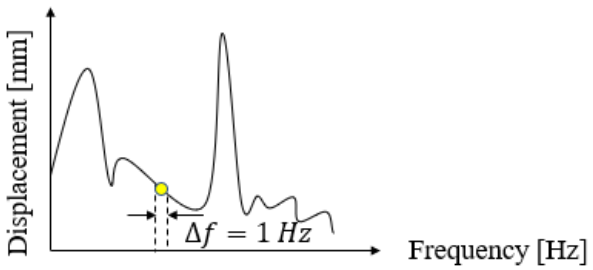

Figure 2.21: Bandpass filter with $\Delta f = 1$ Hz

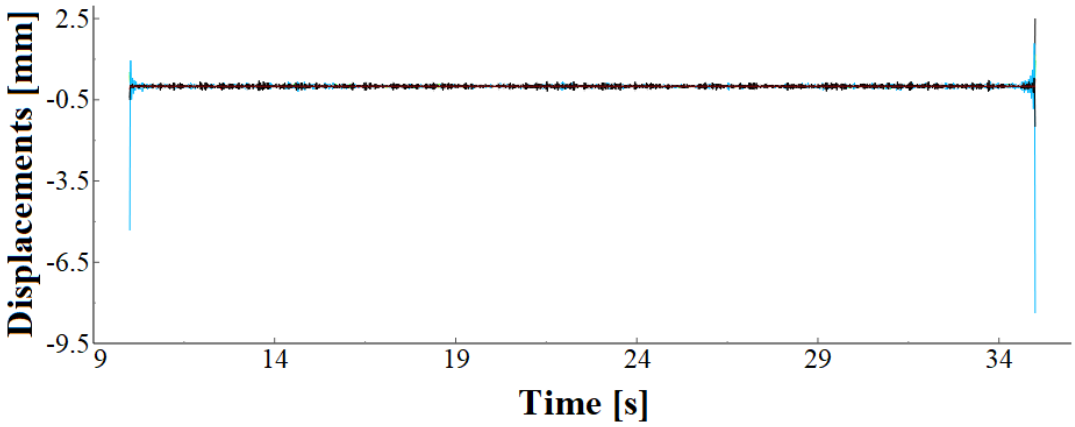

Figure 2.22: Spectral leakage result in deviation at the beginning and end of the time signal

2.11 Rigid body motion

A body can translate or rotate as a whole without undergoing deformation if there are no outside agent that restricts the motion of the body. This is called rigid body motion, defined as combinations of RBM. The physical vehicle clearly possesses a number of RBMs that act during the test. However, these RBMs are not included in the simulation. The RBMs are not included since only the structural deformations are taken into account making body rig simulation. Thus, the contribution of the RBM occurring in the test must be separated in order to enable comparison between the simulation and physical test.

Additionally, the car possesses structural flexible-body modes at frequencies above 10 Hz. Thus, the physical test response data will contain contribution from both of rigid body and flexible-body motion.

The car was subjected to both large and small rigid body motion, superimposed to the flexible structural motion. Large rigid body motion leads to large nodal displacements. Such displacements leads to that ΔD differs greatly from Δz. Unfortunately, a comparison between ΔD and Δz cannot reveal small rigid body motion.

The components within the vehicle are mainly subjected to four specific rigid body motions: pitch, roll, yaw and heave. The pitch mode occurs when the vehicle undergoes rotation around global Y, a roll occurs during rotation around global X and a yaw occurs during rotation around global Z. The heave mode occurs when the vehicle is subjected to pure translation along the global Z coordinate.

2.12 Rigid body motion simulated in Adams

The Chassis & Powertrain Dynamic CAE group at CEVT has initiated a study to identify and map rigid body motion in the complete vehicle simulation using Adams. The complete vehicle simulation shows that the body and powertrain components move in phase with respect to each for excitation below 5 Hz. The group found powertrain out-of-phase modes between 5-10 Hz and wheel suspension modes between 10-20 Hz. The mode responses due to excitation at different frequencies are summarised in Table 2.2.

The Adams model is linearized around the state given by gravity loadings. However, the stiffness of the vehicle body will increase when subjected to heavy road load. Thus, the undamped frequencies will increase when linearization is performed at an arbitrary heavy load case, such as the loads inflicting the vehicle due to severe road conditions.

The modes in Table 2.2 are primary related to different components within the vehicle. Such are the engine pitch and vertical motion which will also cause the remainging body to undergo a pitch motion. A body pitch mode will also occur due to rear wheel parallel modes. However, the mass of rear wheel suspension is less than the mass of the powertrain and the coupling is less strong. Thus, the body pitch modes caused by the powertrain are bigger than the body pitch modes caused by the rear suspension.

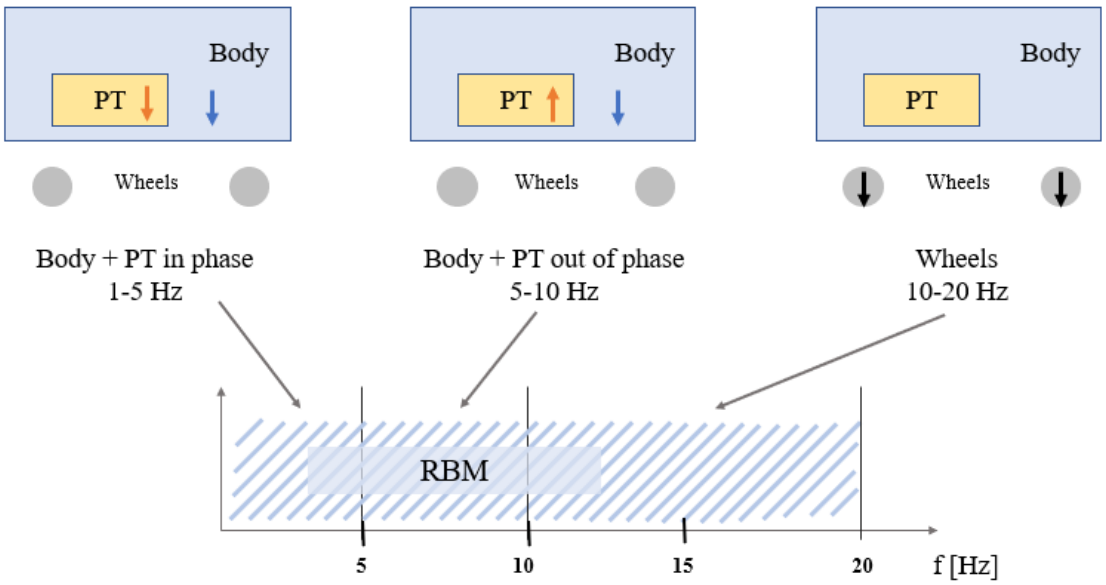

Figure 2.23: Schematic motion and expected RBM in a complete vehicle simulation and physical test.

Table 2.2: Modes at varying undamped natural frequencies

Undamped natural frequency [Hz]	**Modes**
1.6	Body Heave
1.7	Body Roll
2.0	Body Pitch
2.5	Body Yaw
4.4	Body Roll
6.4	Engine Longitudinal
6.6	Engine Lateral
7.7	Engine Pitch
7.9	Engine Pitch
8.2	Engine Pitch/Yaw
9.6	Engine Vertical
9.7	Engine Yaw
10.7	Rear wheel Opposite Longitudinal
11.5	Rear wheel Parallell Longitudinal
11.6	Engine Roll
16.5	Rear Wheel Parallell Vertical
16.6	Front Wheel Opposite Vertical
17.3	Front Wheel Opposite Vertical
17.4	Front Wheel Parallell Vertical
20.0	Front Wheel Steering

3
Methods

The methodology behind the complete vehicle simulation and the data processing is presented in following section.

3.1 Complete vehicle simulation

The complete vehicle simulation was executed using different computer software. The procedure is explained step by step below.

3.1.1 Meta

The computer software Meta has a build in "script editor" tool. This tool was used to automatise the post-processing procedure with the help of different python scripts. Moreover, Meta was used to animate the eigenmodes of the car. The eigenmodes study was executed to investigate the type of modes appearing at different frequencies, such as torsion, bending, pump or local mode. Lastly, Meta was used to visualise and export results in terms of pictures, animations and text files.

3.1.2 Body rig simulation

The body rig simulation was executed in order to compute the relative displacement for all closure openings and to study the eigenmodes of the car. The input for the complete vehicle simulation was the multi-stethoscope, load case prescription, coordinate system definition and a modal damping value.

3.2 Data processing

The physical test data was originally in csv format, containing the acceleration in global coordinates. The simulation data on the other hand was in pch format, containing the displacement in global coordinates. As a result, the physical test data had to be processed by converting it from csv to pch format. A numerical integration from acceleration to displacement was performed and time data was cut to an appropriate duration. A coordinate transformation was performed in order to compute the relative displacement and furthermore, the data processing for the simulation data required time cutting and a coordinate transformation. A chart of the data processing procedure is demonstrated in Figure 3.1.

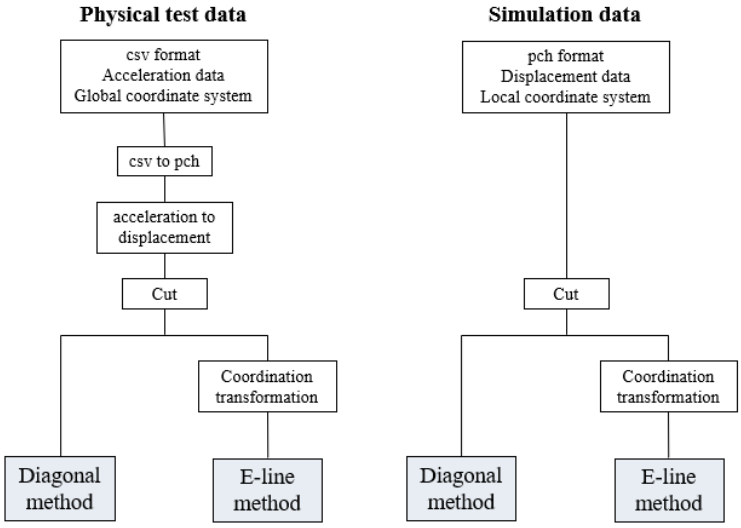

Figure 3.1: Data processing procedure for physical test and simulation data

3.3 Python tools

The python scripts used are presented below. Several of the scripts presented below were developed by CEVT.

3.3.1 Time-select

The "time select" tool, developed by Jacobsson and Jörrud, was used to cut the data for a specific time sequence. The input to the program was a pch file containing data in time domain. Once the program is run, a pop-up window asks for a time interval to cut out, see Figure 3.2. The output was a pch file containing the reduced time domain data [2].

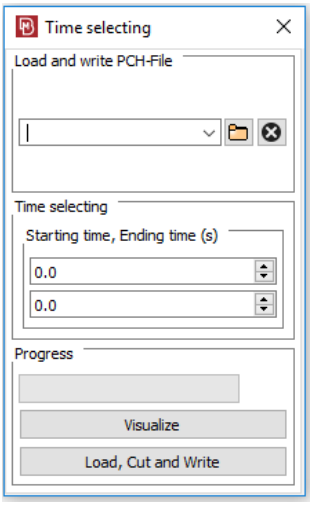

Figure 3.2: Time selecting tool pop up window

3.3.2 Spectral leakage

Spectral leakage was identified by studying the differences between reverse and forward cumulative, bandpass and cut-off SEP filtered signals. The signal was free from spectral leakage if the reverse and forward filtering presented identical results. Additionally, all comparison filter scripts have a build-in signal cutter which excludes the 0.5 first and last seconds of the filtered signal. The purpose was to prevent spectrum leakage effects at the beginning and end of the time sequence.

3.3.3 Coordination transformation

The physical test and simulation data were provided in global coordinate system. Therefore, the "coordination transformation" tool was used to transform the coordinates from a global to a local coordinate system.

3.3.4 Filtering

The FFT operation was performed using the integrated Meta tool "ideal bandpass filter" where a certain frequency interval was chosen. This procedure was implemented and automized in respective comparison filter script. The algorithms for the three comparison filters were programmed according to the procedures described in Sections 2.10.1-2.10.2. Furthermore, the iFFT process was performed using the Python script "filtering". The input to the program was the time domain signal and a requested cut-on frequency. The output from the program was filtered data in time domain. This procedure was used when the data was studied in time domain for a specific frequency interval.

3.3.5 E-line method

The "E-line method" tool was scripted to require pch file in local coordinate system as input. The script was programmed to compute the relative displacement according to equations (2.17) - (2.19) for each time step and node pair. Lastly, the script provided the user with a pch file which contains all relative displacements for a specific SEP value. The pch file contains the result for each time step and node pair.

3.3.6 Diagonal method

The script structure of the "Diagonal method" tool bears resemblance to the structure of the "E-line method" tool. The required input file was also in pch format, but in global coordinate system. However, the diagonal method tool was scripted according to equation (2.21). The values for x_0, y_0, z_0 and D_0 was obtained using the measurement tool in Ansa. Lastly, the script was programmed to return a pch file containing all relative displacements for each time step and node pair.

4
Results

The correlation results between the physical test and the complete vehicle simulation are presented in this section. The initial part of the results aims to identify large displacement and to study the global motion of the car. The wheel forces are then studied to ensure that similar load level is subjected during both simulation and physical test. The second part of the result aim to detect contributing modes by studying the cumulative filter plots. The final part of the result focus on the actual correlation study for varying impact parameters.

4.1 Identifying large displacements

The first correlation step is to identify large displacements. These displacements can be identified by comparing the relative displacements ΔD and Δz, see section 2.7. The structure will not be exposed to large deformations if ΔD is equal to Δz. The displacement ΔD and Δz for physical test when driving on PAV at 50 km/h is presented in Figure 4.1.

The difference between ΔD and Δz is negligible according to Figure 4.1. Thus, the physical test data does not contain large deformations, but may contain a combination of small RBM and structural deformation. The results are obtained for all load cases. The correlation study following this section will therefore be proceeded using Δz.

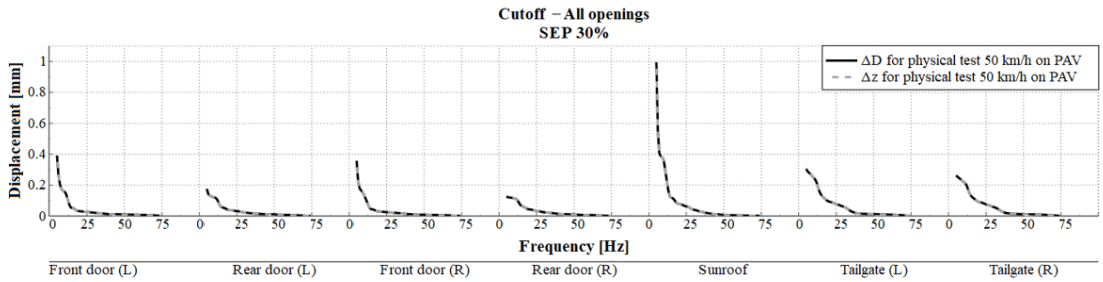

Figure 4.1: Cut-off filter applied to all closure openings of the car with SEP 30% value for ΔD and Δz. Test speed 50 km/h on PAV.

4.2 Global motion identification

This section reports a study of the global motion of the car. This will be done by comparing physical test and simulation with respect to Δx and Δy. The relative displacements Δx and Δy for physical test and simulation with a modal damping factor of 2% when driving on WOP at 50 km/h are presented in Figures 4.2-4.3. Whereas the relative displacements Δx and Δy for physical test and simulation with 2% modal damping when driving on WIP at 50 km/h, see Figures 4.2-4.3.

Δx is six times higher at the tailgate in comparison with the door openings, according to Figure 4.2. The peaks at the tailgate occur at 10 Hz. The simulation is clearly under-predicting the mode response at the tailgate when comparing it with physical test, while the difference between simulation and physical test is significantly less at the doors.

The relative displacement Δy at the doors shown in Figure 4.3 peaks at 10 Hz for the physical test. The displacement is higher for the front doors in comparison with the rear doors. The difference occurs because the distance in local z between the master and slave nodes is smaller in rear door than in the front door. The displacements at the tailgates are about one third of the displacements at the front doors. Additionally, the displacement at the doors for the physical test is 4-6 times higher than shown by simulation data.

All major peaks in Figure 4.2-4.3 occur at the same frequency and are solely present for the physical test. This indicates a strong rigid body motion contribution. This rigid body motion is most likely a roll mode as evident by that the highest Δx displacement occurs at the tailgate and the highest Δy displacement occurs at the side doors, see the multi-stethoscope in Figure 2.7.

The displacement Δx is highest at the doors according to Figure 4.4. The relative displacement for each door opening consist of two distinct peaks, where the peaks at the front doors is higher than at the rear doors. The first and second peak occurs at 7 respective 12 Hz for all door openings.

The displacement Δy is higher at the tailgate in comparison with the doors according to Figure 4.5. The relative displacement Δy for tailgate also consist of two distinct peaks, where the first and second peak occurs at 7 respectively 12 Hz. Additionally, the relative displacement at the front door is slightly higher than at the rear door.

The major double peaks in Figures 4.4-4.5 occur in the same frequency range and are solely present for the physical test. This indicates two rigid body motions. The most strongly rigid body motion is a pitch mode as evident by that the highest Δx displacement occurs in the side doors and the highest Δy displacement occurs at the tailgate, see Figure 2.7 for further details.

The displacement caused by frequencies below 5 Hz cannot be studied in the physical test as the accelerometers are not accurate enough at these low frequencies. Thus, the body and powertrain in phase modes occurring in a vehicle cannot be identified, see Figure 2.23. Additionally, the two pitch and roll modes identified in physical test are most likely caused by powertrain out-of-phase modes. Lastly, the heave and roll modes caused by wheel suspensions are less distinct than the heave and roll modes caused by the powertrain out-of-phase modes, since the mass of rear wheel suspension is less than the mass of the powertrain.

In conclusion, the simulation clearly under-predicts data at specific frequencies below 20 Hz for all load cases and closure openings. Data from test are significantly larger. This indicates that the physical test data is impacted by rigid body motions. The simulation contains only structural modes. Thus, the rigid body modes occurring in physical test must be identified and excluded from the structural modes in order to enable a comparison between simulation and test. Hence, the correlation study following this section will solely include frequencies above 20 Hz in order to only compare structural modes. See the global motion identifying study for remaining load cases in Figures B.1-B.2 in Appendix B.

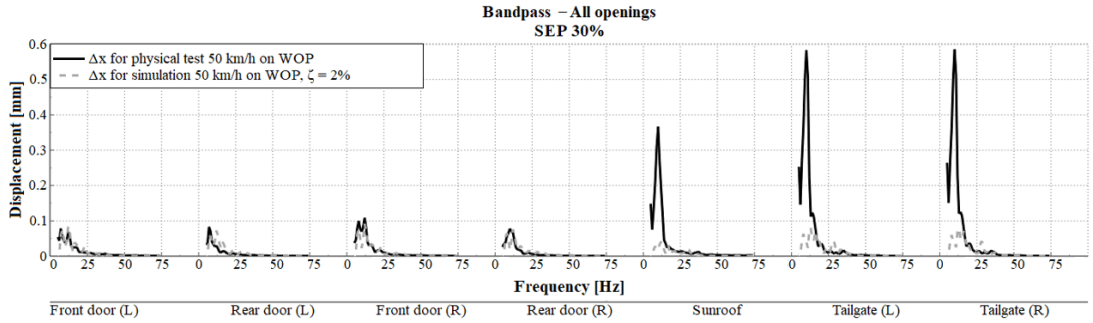

Figure 4.2: Bandpass filter applied on all closure openings of the car with SEP 30% value for Δx. Physical test speed 50 km/h and simulation speed 50 km/h with $\xi = 2\%$ driving on WOP.

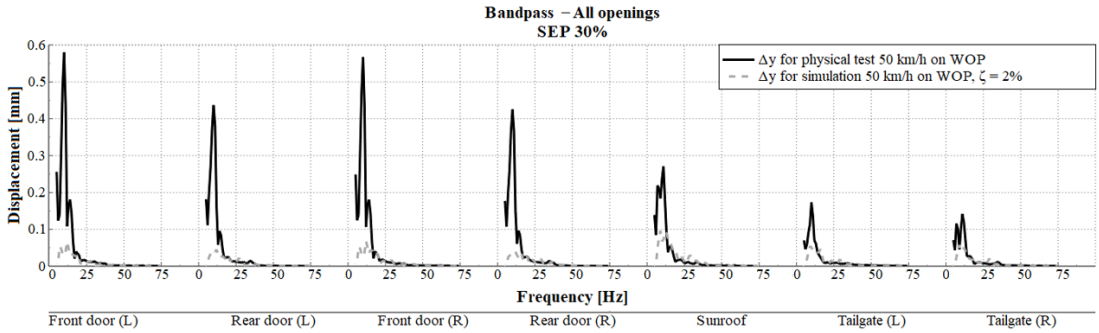

Figure 4.3: Bandpass filter applied on all closure openings of the car with SEP 30% value for Δy. Physical test speed 50 km/h and simulation speed 50 km/h with $\xi = 2\%$ driving on WOP.

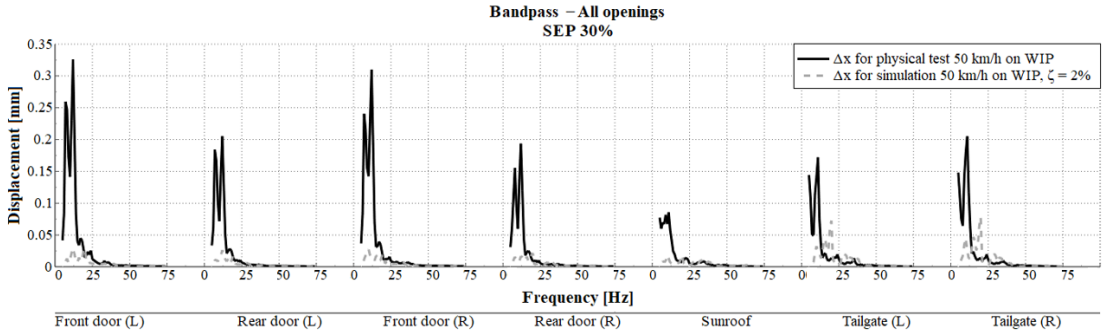

Figure 4.4: Bandpass filter applied on all closure openings of the car with SEP 30% value for Δx. Physical test speed 50 km/h and simulation speed 50 km/h with $\xi = 2\%$ driving on WIP.

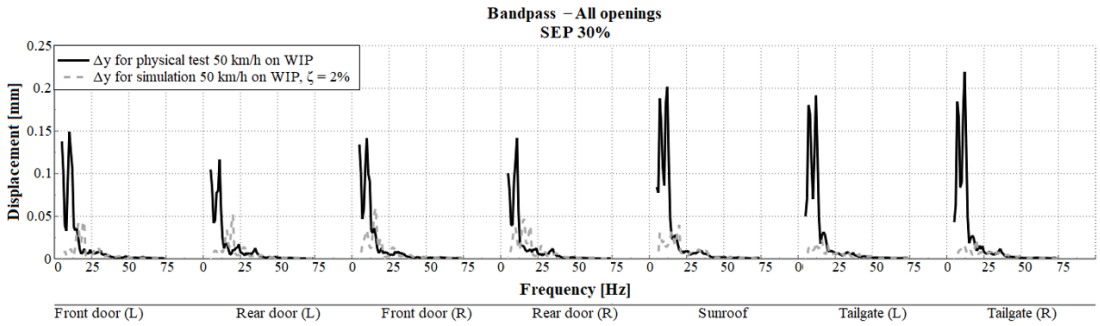

Figure 4.5: Bandpass filter applied on all closure openings of the car with SEP 30% value for Δy. Physical test speed 50 km/h and simulation speed 50 km/h with $\xi = 2\%$ driving on WIP.

4.3 Wheel force

It is important to compare the load level in test and simulation before performing the actual correlation study. The magnitude of the wheel force is observed for both physical test using the WFT and simulation using Ftire. The force for the front right wheel in z direction is presented in Figure 4.6.

The magnitude of the force is highest for PAV according to Figure 4.6. However, it is not enough to solely study the magnitude of the forces to conclude which track and velocity that contributes to the highest wheel force. The RMS value is calculated for each track in order to make the wheel forces obtained from physical test and Adams simulation comparable, see Table 4.1 for The RMS values.

The results presented in Table 4.1 presents a very good correlation between physical test and simulation. The following observations are made studying Table 4.1: The RMS value increases with increased velocity for WIP and WOP, which is expected.

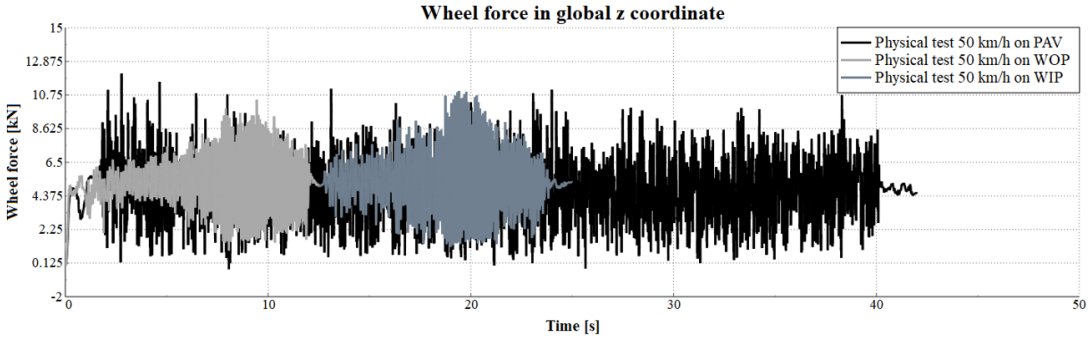

Figure 4.6: Wheel force in z for physical test speed 50 km/h driving on PAV, WOP and WIP

Table 4.1: The RMS value for physical test and simulation for each load case, including the percentile difference between simulation and physical test.

Tracks and velocity	Physical test [kN]	Simulation [kN]	Percentile difference between simulation and physical test
WIP 50 km/h	5.524	5.288	-4%
WIP 30 km/h	5.320	5.123	-4%
WOP 50 km/h	5.357	5.179	-3%
WOP 30 km/h	5.295	5.125	-3%
PAV 50 km/h	5.013	4.727	-6%
PAV 30 km/h	5.355	5.248	-2%

However, the RMS value decreases when increasing the velocity for PAV. A possible explanation is that the wheels loses road grip, as the car wheels jumps over the stones. This causes higher force magnitudes when the car wheels eventually hits a single stone. The same phenomenon can be seen in both test and simulation data.

The correlation study can now be proceeded focusing on the opening distortion. See Figure C.1 in Appendix C for the wheel force when driving at 30 km/h.

4.4 Identifying contributing frequency with help of a cumulative filter

The cumulative filter is performed in order to identify the most contributing frequencies. This procedure is applied on both simulation and physical test data for all load cases. The results for WOP road condition are presented in Figure 4.7.

The frequency contribution with respect to the displacement is less than 1% after 50 Hz according to Figure 4.7. The most contributing frequencies are located below 50 Hz. The cumulative filter for PAV and WIP is presented in Figures D.1-D.2 in Appendix D. These tracks presented similar tendency as in Figure 4.7. In order to

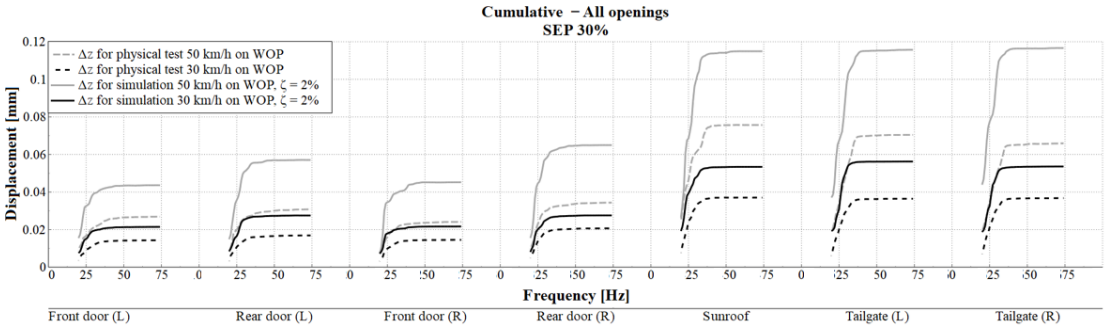

Figure 4.7: Cumulative filter applied on all closure openings of the car with SEP 30% value for Δz. Physical test speed 50 km/h, physical test 30 km/h, simulation speed 50 km/h with $\xi = 2\%$ and simulation 30 km/h with $\xi = 2\%$ driving on WOP.

only focus on the most contributing modes during the correlation study the frequencies between 50 and 75 Hz will be hidden in the plots.

4.5 Correlation with respect to varying parameters

The purpose with the following section is to study the impact of varying parameters on the correlation between physical test and simulation data. The impact of the various tracks is studied in order to determine if, and if so in which manner, the varying tracks influences the result. The velocity impact is studied by first defining an offset value between 30 km/h and 50 km/h for both physical test and simulation. The offset value is based on a visual best fit when scaling down the curve for 50 km/h for all openings. The last studied parameter is the damping. The purpose is to determine which modal damping that gives best correlation with physical test results.

All parameter studies are performed using the cut-off plot presenting the frequencies between 20-75 Hz. All studies are performed using a filter with 30% SEP value. Moreover, the displacement is computed in local z direction. The correlation study is extensive and includes several load cases within each parameter study. As a result, many load cases that add to the illustration of already observed results are presented in Appendix A-G.

4.5.1 Track load influence

The influence of various tracks is investigated in following subsection. The relative displacement Δz for both physical test and simulation when driving on all tracks at 50 km/h is presented in Figures 4.8-4.9.

The relative displacement for WOP and WIP is slightly higher at the doors according to Figure 4.8. However, the relative displacement difference between WOP and WIP is considerably higher at the tailgate opening. This is reasonable because the WOP causes torsion at the tailgate opening, which clearly increases the displacement.

There is a relative displacement difference between WOP and WIP at the doors according to Figure 4.9. However, the relative displacement difference between WOP and WIP is considerably higher at the tailgate opening.

The rear doors are subjected to larger deformations than the front doors, this pattern is observed in both simulation and physical test. One possible explanation is that the A-pillar is a closed section, while B and C-pillars are open sections. This contributes to additional stiffness at the front door, thus reducing the displacement further.

Additionally, the tailgate opening is exposed to higher relative displacements than remaining openings when driving on WOP and PAV in both simulation and physical test. The larger displacement at the tailgate is likely caused by the torsion inflicted by the WOP and PAV tracks. Lastly, the PAV contributed to the highest distortion in all load cases, which is expected since PAV generates the highest wheel forces. The relative displacement Δz for both physical test and simulation when driving on all tracks at 30 km/h displayed similar result, see Figures E.1-E.2 in Appendix E for further details.

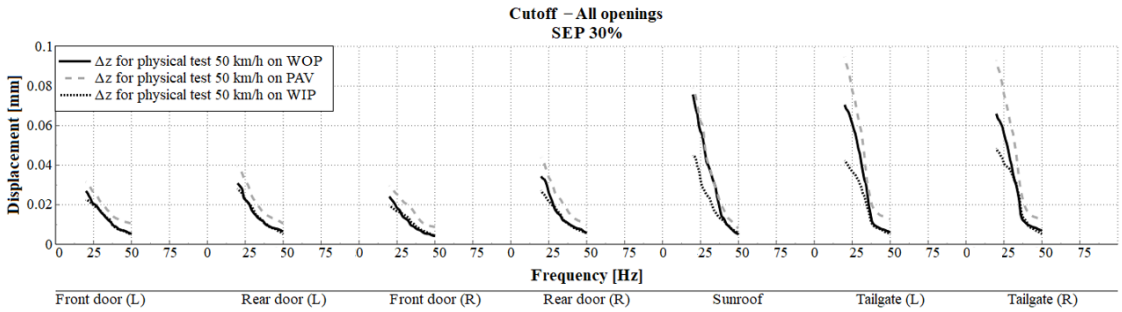

Figure 4.8: Cut-off filter applied on all closure openings of the car with SEP 30% value for Δz. Physical test speed 50 km/h driving on WOP, PAV and WIP.

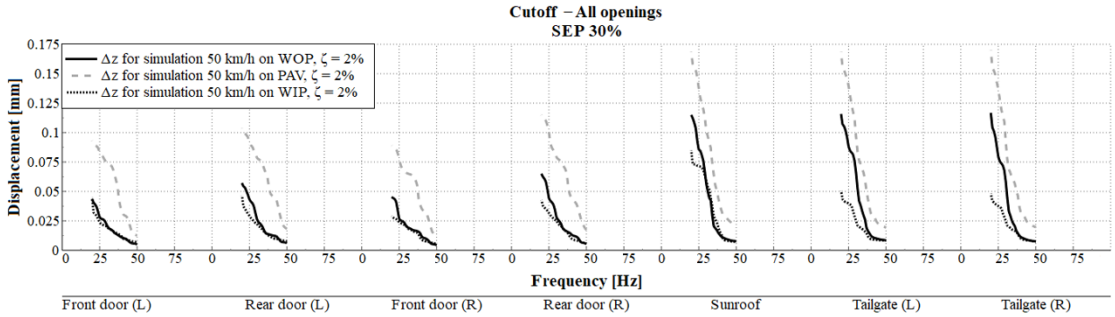

Figure 4.9: Cut-off filter applied on all closure openings of the car with SEP 30% value for Δz. Simulation speed 50 km/h with $\xi = 2\%$ driving on WOP, PAV and WIP.

4.5.2 Velocity influence

By using a rough assessment criteria the velocity influence is major for both physical test and simulation results. The distortion values for the results from 50 km/h are scaled down to the results from 30 km/h. A visual best fit for all openings is reached. This procedure is done for both physical test and simulation. The scaling factors is presented in Table 4.2. The velocities follows the same pattern at the doors according to Figure 4.10. The relative displacements at the tailgate deviate below 30 Hz.

The 50 km/h case scaled by a factor of 0.45 coincides with the 30 km/h at the doors according to Figure 4.11. The relative displacement deviate below 31 Hz at the tailgate.

One global scaling factor is not enough to represent all closure openings, as seen in Figure 4.12. The scaled results of 50 km/h coincides exceptional well with the results of 30 km/h at high frequencies. The relative displacement at the rear doors and the left side of the tailgate correlates better at low frequencies.

The relative displacement correlation is poor at the tailgate according to Figure 4.13. The relative displacement at the doors shows better correlation. The scaling factors for respective load case are presented in Table 4.2. It can be seen that a velocity increase in physical test results in a similar increase of the relative displacement in simulation.

Table 4.2: Summarise of all scaling factors for respective load cases.

Track	Physical test	Simulation
WOP	0.6	0.45
PAV	0.45	0.55
WIP	0.55	0.45

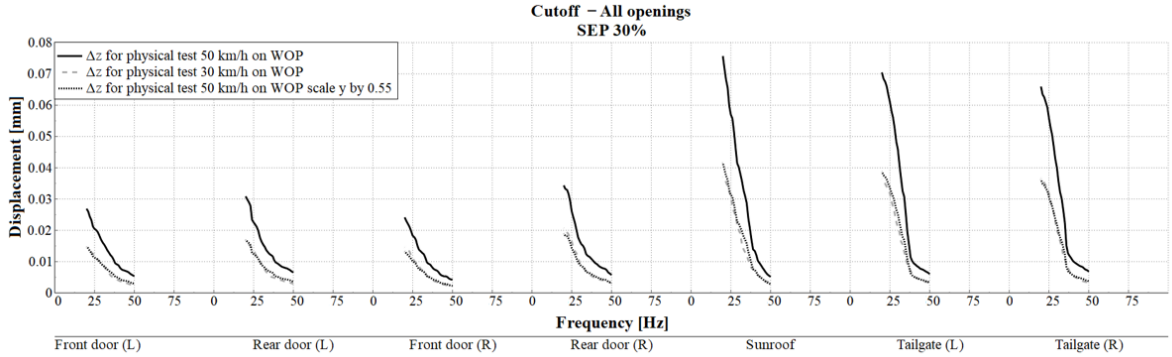

Figure 4.10: Cut-off filter applied on all closure openings of the car with SEP 30% value for Δz. Physical test speed 50 km/h and physical test 30 km/h driving on WOP. The physical test speed 50 km/h is scaled in vertical direction by factor 0.55.

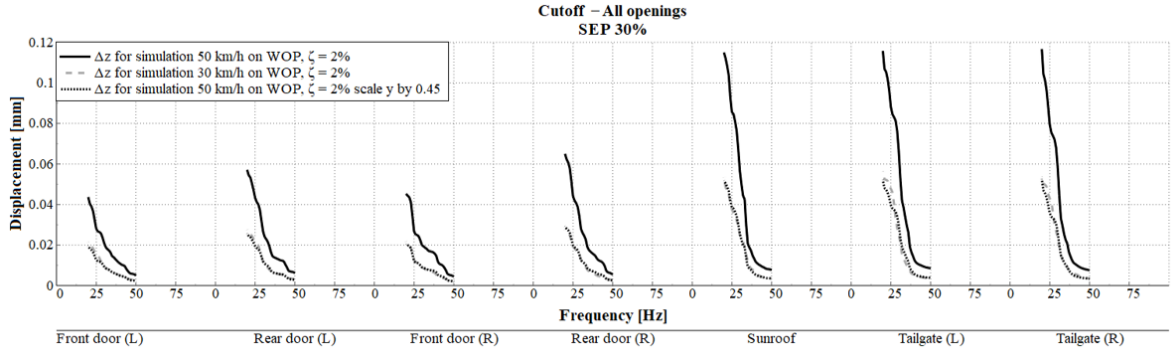

Figure 4.11: Cut-off filter applied on all closure openings of the car with SEP 30% value for Δz. Simulation speed 50 km/h with $\xi = 2\%$ and simulation 30 km/h with $\xi = 2\%$ driving on WOP. The physical test speed 50 km/h is scaled in vertical direction by factor 0.45.

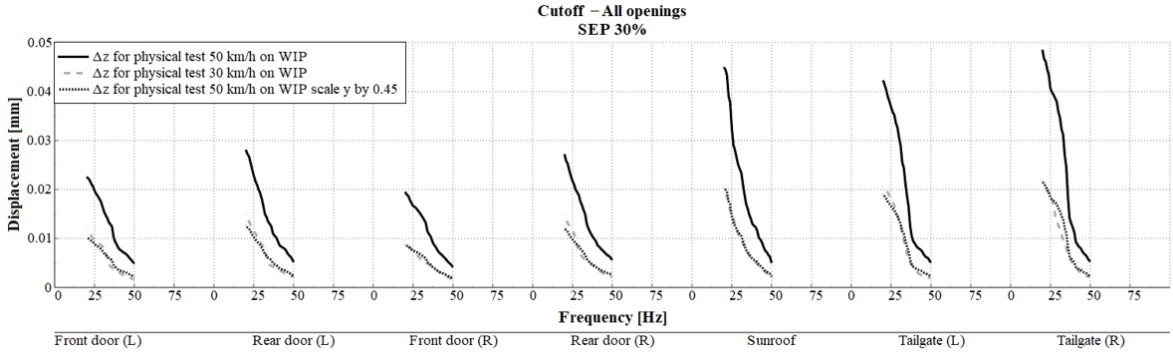

Figure 4.12: Cut-off filter applied on all closure openings of the car with SEP 30% value for Δz. Physical test speed 50 km/h and physical test 30 km/h driving on WIP. The physical test speed 50 km/h is scaled in vertical direction by factor 0.45.

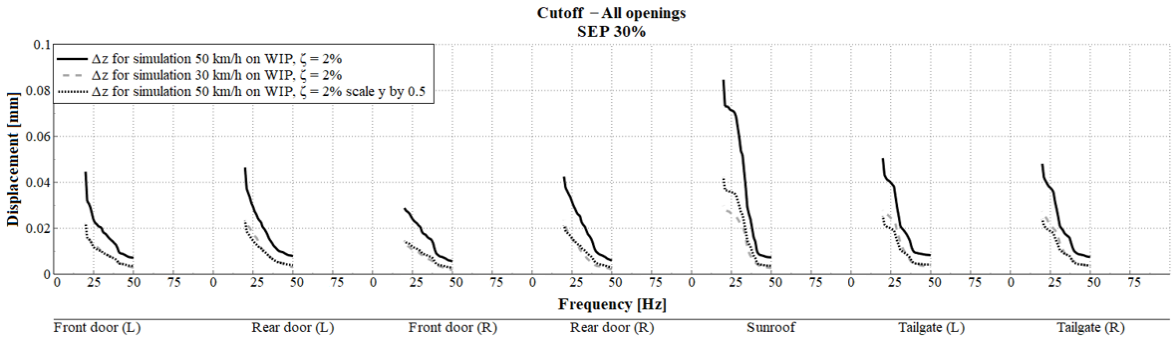

Figure 4.13: Cut-off filter applied on all closure openings of the car with SEP 30% value for Δz. Simulation speed 50 km/h with $\xi = 2\%$ and simulation 30 km/h with $\xi = 2\%$ driving on WOP. The physical test speed 50 km/h is scaled in vertical direction by factor 0.50.

4.5.3 Influence from Damping

The physical test data is compared with two simulation cases: one with 2% modal damping and one with 15% modal damping. This study is performed for both 30 km/h and 50 km/h speeds on all tracks. The purpose is to study the influence of various modal damping speeds.

In conclusion, results from using 15% modal damping bears more resemblance to results obtained in physical test. The correlation is very strong above 40 Hz according to Figure 4.14. The simulation data with 2% modal damping generally predict higher relative displacement than those observed in physical test.

Figure 4.15 shows that simulation with 2% modal damping give results that coincides with physical test data above 30 Hz at the tailgate. This behaviour is similar to that of the right front and rear door as well, but them for frequencies above 40 Hz. The physical test result for the left front and rear door is better described by simulation with 15% modal damping at frequencies above 20 Hz.

The physical test results for the tailgate correlates very well with the 2% modal damping case above 30 Hz according to Figure 4.16. The simulation results with 15% modal damping correlates better for low frequencies at the rear doors. The relative displacement correlation is poor at the tailgate with both 2% and 15% modal damping case, according to Figure 4.18. The relative displacement for simulation with 2% modal damping value gave over-prediction to physical test at all closure openings.

The relative displacement at the tailgate for the simulation with 2% modal damping gives a response more similar to physical test, according to Figure 4.18. The simulation with 15% modal damping is clearly under-predicting physical test at all closure openings. Simulation with 2% modal damping bears resemblance with physical test at high frequencies. Whereas results from simulation data with 15% modal damping

is preferable at low frequencies since it resembles with the results from physical test more than the results from simulation data with 2% modal damping.

Analysing Figure 4.19 it can be observed that simulation with 2% modal damping gives better results with physical test at high frequencies. This statement is valid for all closure openings. As the frequency decreases the results from the simulation data with 15% modal damping correlates best with physical test.

The difference between the results in Figures 4.14-4.16 are large when studying the modal damping influence. It is difficult to draw a conclusions of which modal damping value is suitable since the results for different road load varies. The difference between the 2% and 15% damping case is immense at lower frequencies. The simulation results with 15% modal damping is more similar to the results from physical test at low frequencies, whereas the results from simulation with 2% modal damping is similar to physical test results at high frequencies. This behaviour is observed in the door opening for WOP and WIP at 50 km/h.

The amplitude of forces are reduced with help av a damping factor. These forces affects the displacement, consequently. As a result, the displacement response is reduced with help of a modal damper. Additionally, similarities between physical test and high damping indicates a more dynamic response, while similarities between physical test and lower damping indicates a more static response. Thus, a good correlation between simulation with high damping factors and physical test may indicate poorly modelled modes.

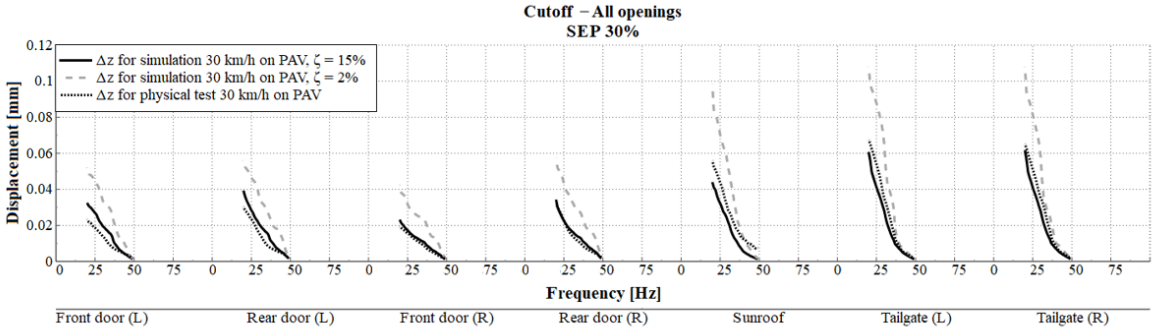

Figure 4.14: Cut-off filter applied on all closure openings of the car with SEP 30% value for Δz. Simulation 30 km/h with $\xi = 2\%$, simulation 30 km/h with $\xi = 15\%$ and physical test 30 km/h driving on PAV.

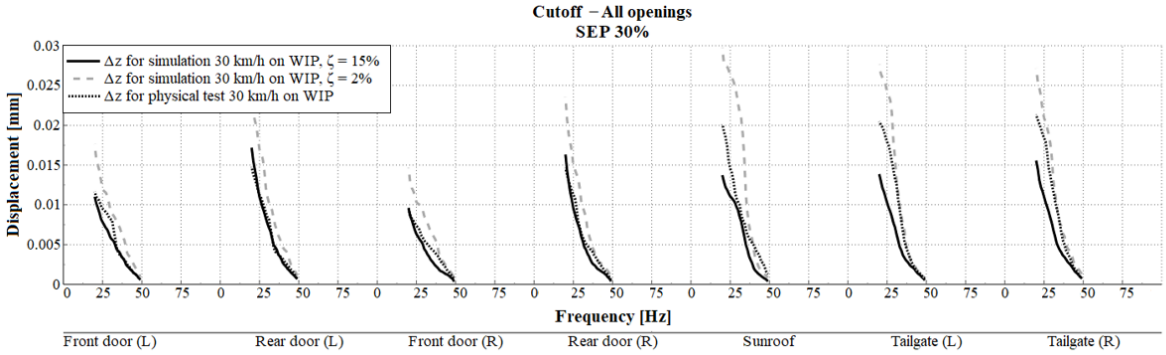

Figure 4.15: Cut-off filter applied on all closure openings of the car with SEP 30% value for Δz. Simulation 30 km/h with $\xi = 2\%$, simulation 30 km/h with $\xi = 15\%$ and physical test 30 km/h driving on WIP.

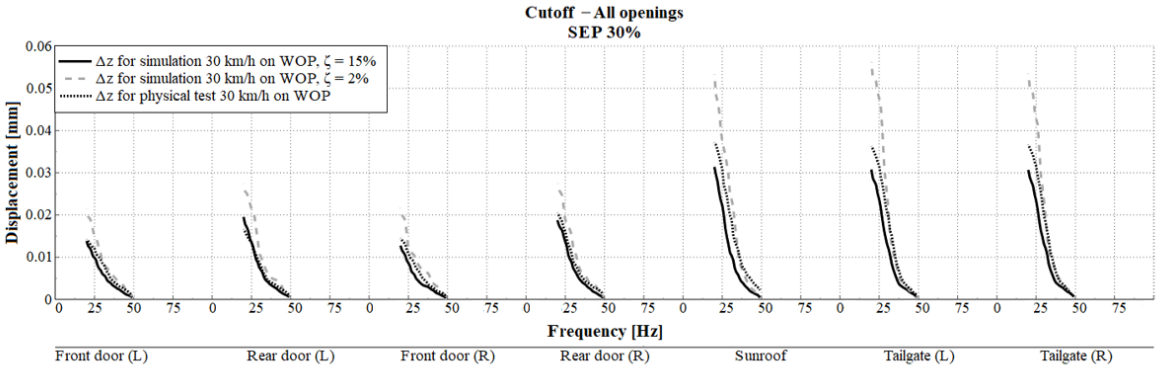

Figure 4.16: Cut-off filter applied on all closure openings of the car with SEP 30% value for Δz. Simulation 30 km/h with $\xi = 2\%$, simulation 30 km/h with $\xi = 15\%$ and physical test 30 km/h driving on WOP.

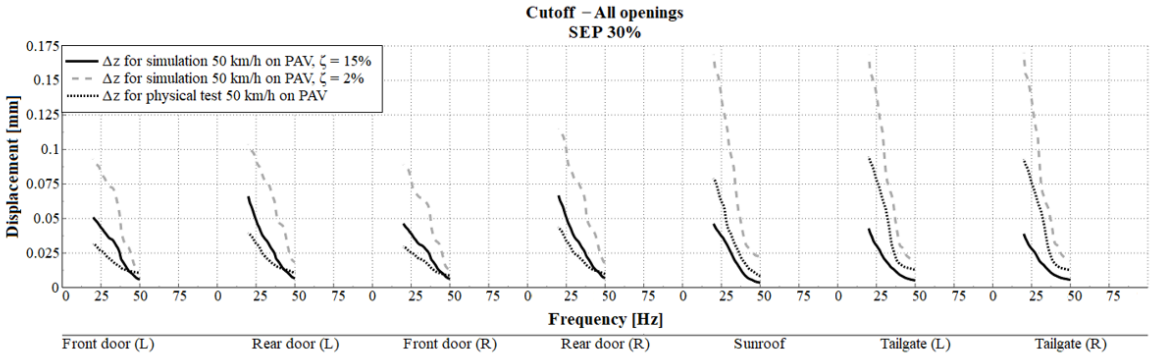

Figure 4.17: Cut-off filter applied on all closure openings of the car with SEP 30% value for Δz. Simulation speed 50 km/h with $\xi = 2\%$, simulation speed 50 km/h with $\xi = 15\%$ and physical test speed 50 km/h driving on PAV.

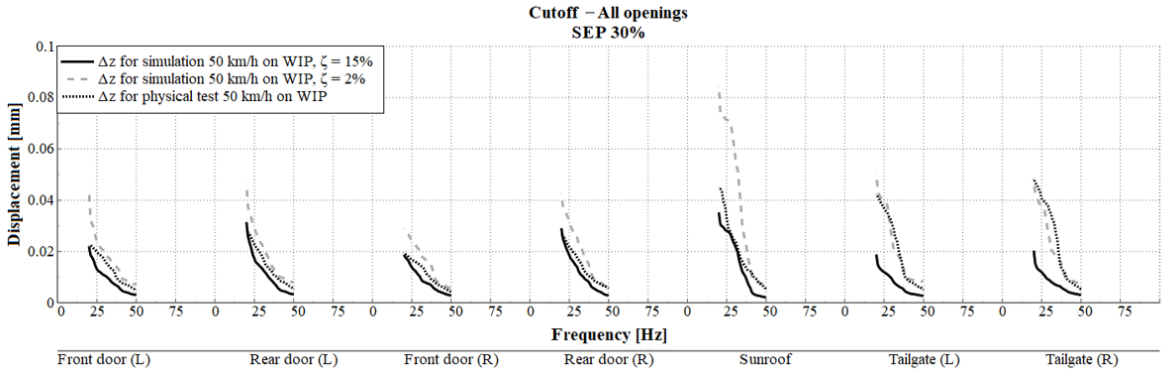

Figure 4.18: Cut-off filter applied on all closure openings of the car with SEP 30% value for Δz. Simulation speed 50 km/h with $\xi = 2\%$, simulation speed 50 km/h with $\xi = 15\%$ and physical test speed 50 km/h driving on WIP.

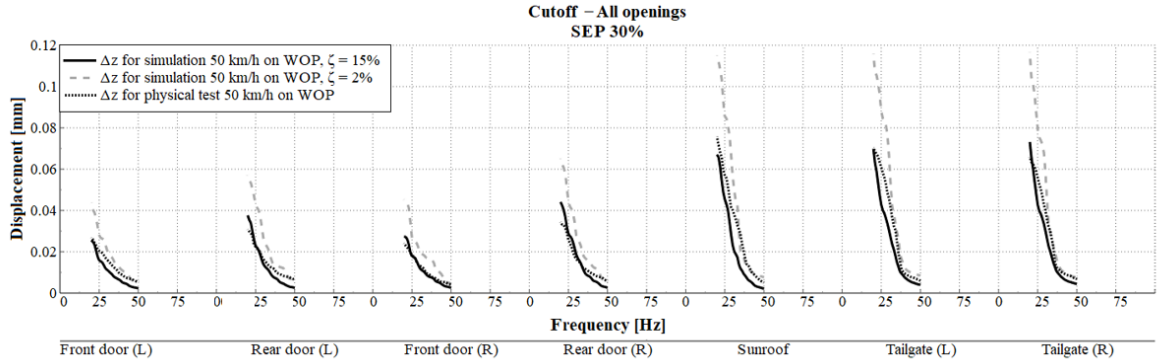

Figure 4.19: Cut-off filter applied on all closure openings of the car with SEP 30% value for Δz. Simulation speed 50 km/h with $\xi = 2\%$, simulation speed 50 km/h with $\xi = 15\%$ and physical test speed 50 km/h driving on WOP.

4.6 Component per opening

In this section the local component for each opening is studied more in detail. The relation between the components indicates how good the simulation modell is capturing the overall body stiffness.

The relative displacement results Δy is higher than the results for Δx and Δz at the front doors for both physical test and simulation according to Figure 4.20. Δx is higher than Δz at the front doors. The tailgate presents the opposite results. Δz is the dominant component for physical test and simulation. The Δz displacement obtained from simulation is over-predicting physical test at the rear doors. This observation can be seen when driving 30 km/h on PAV, see Figure G.1.

The relative displacement Δx, Δy and Δz at the tailgate presented similar behaviour between the results from simulation and physical test according to Figure

4.21. The relative displacement Δx for simulation is slightly over-predicting in physical test at the tailgate, while Δy and Δz are under-predicting. Analysing the three components for the side doors it can be observed that the results for Δy in simulation is under-predicting the results physical test. This can be due to local eigenmodes caused by the front and rear seats in the complete vehicle simulation. This observation can also be seen when driving at 30 km/h on WOP, see Figure G.2.

Analysing the results presented in Figure 4.22 it can be observed that the complete vehicle simulation results did not capture the same local component pattern as in the results for physical test in all openings.

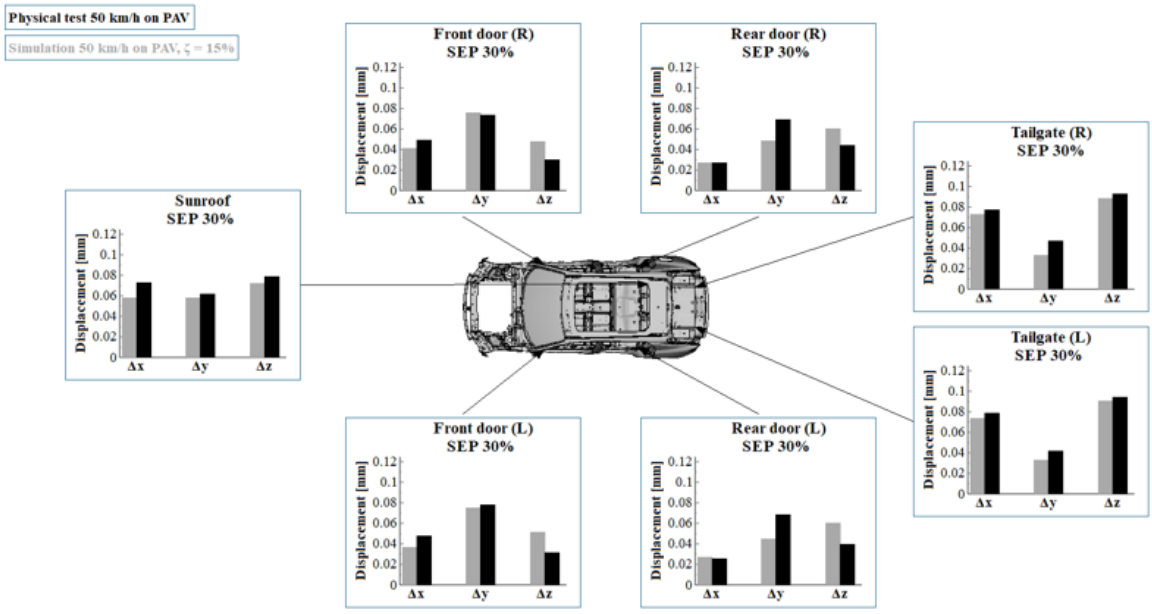

Figure 4.20: Mean value applied on all closure openings of the car with SEP 30% value for Δx, Δy and Δz for physical test speed 50 km/h and simulation speed 50 km/h with $\xi = 15\%$ driving on PAV

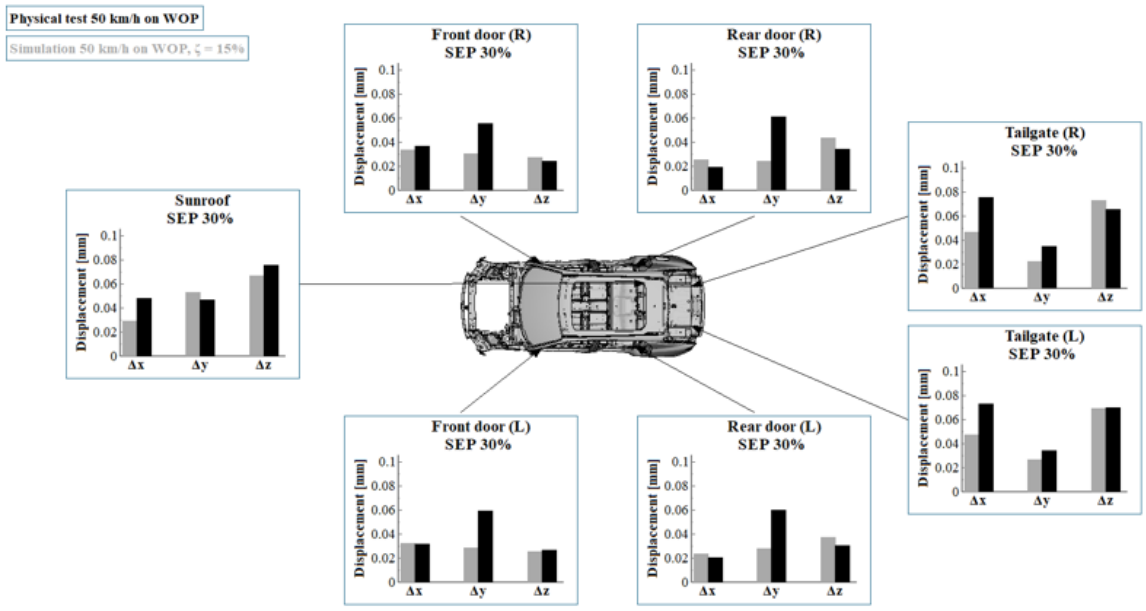

Figure 4.21: Mean value applied on all closure openings of the car with SEP 30% value for Δx, Δy and Δz for physical test speed 50 km/h and simulation speed 50 km/h with $\xi = 15\%$ driving on WOP

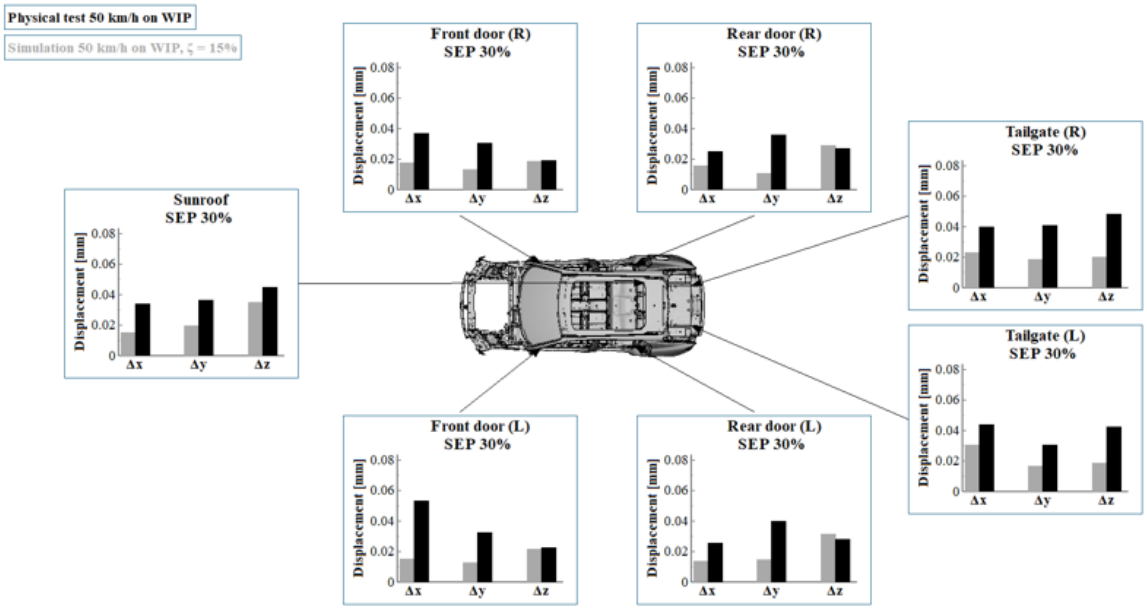

Figure 4.22: Mean value applied on all closure openings of the car with SEP 30% value for Δx, Δy and Δz for physical test speed 50 km/h and simulation speed 50 km/h with $\xi = 15\%$ driving on WIP

5
Concluding Remarks

The purpose with this section is to draw conclusions from the presented results. In addition future work is suggested.

5.1 Conclusion from results

A post processing procedure is developed which made the complete vehicle testing and body rig simulation data comparable.

The physical test contain rigid body motion, whereas the simulation data solely include the displacement caused by structural deformations. Thus, the RBM occurring in physical test must be identified and excluded from the structural modes in order to enable a comparison between simulation and test.

The relative displacements Δz and ΔD are compared for physical test data. The results obtained above 5 Hz indicates that none of the load cases subjects the vehicle to large rotations and therefore Δz and ΔD are more-or-less equal. However, the physical test still include small RBM. These modes are captured studying the global motion of the car. One roll and two pitch modes are clearly identified between 5-10 Hz. These three modes are likely caused by body and powertrain out-of-phase modes. However, the body motion caused by the body and powertrain out-of-phase mode is more distinct than the body motion caused by the wheel suspension modes. As a result, the displacement caused by the wheel suspension modes may be difficult to distinguish from structural modes, as the displacement caused by wheel suspension mode is less prominent than the displacement caused by body and powertrain modes. A cutoff frequency at 20 Hz is introduced in order to diminish the effect of all rigid body motion, including the modes caused by wheel suspension modes. In conclusion, the physical test and simulation are now comparable since both data signals are dominated by flexible modes.

Furthermore, the most contributing frequencies is observed to be located below 50 Hz according to the cumulative plot, as the mode contribution is less than 1% for frequencies above 50 Hz. However, the mode contribution due to frequencies between 50-75 Hz are included in the analysis, but do not produce visible results in the graphs.

The wheel forces were compared between simulation and test before starting the

actual correlation study. The results presented a good correlation between simulation and physical test based on evaluating the RMS value of the forces. That make the correlation study more thrustworthy since the same load levels is obtained from both physical test and simulation. Further evaluation of the RMS gave following side observation: an increased velocity when driving on WIP and WOP results in increased RMS values, whereas the RMS values decreased when driving on PAV. One possible explanation could be that the wheels follows the bumps when driving at 30 km/h for all road conditions. This occur when driving at 50 km/h on WIP and WOP. However, the wheels loses their road grip, as the car wheels make larger jumps over the stones of the PAV, when the velocity increases. This causes high force magnitudes when the car eventually lands on the track but in effect leads to decreased RMS value when the velocity increases.

The actual correlation included studying the influence of various tracks, velocities and dampings in simulation and when possible physical test.

A number of observations are made during the track correlation investigation. For instance, the rear doors are subjected to larger relative deformations than the front doors. One possible explanation is that the A-pillar is a closed section, while B and C-pillars are open sections. This contributes to additional stiffness at the front door, thus reducing the relative displacement. Additionally, the tailgate opening is exposed to higher relative displacements than the remaining openings when driving on WOP and PAV. The increased increment at the tailgate is likely caused by the torsion inflicted by the WOP and PAV tracks. Furthermore, driving on PAV gave higher displacement. This observation is expected as the PAV contributed to the largest wheel forces.

The second studied parameter was the velocity influence on the relative displacements. The relative displacements increased when the velocity increased from 30 km/h to 50 km/h for all test tracks, which is expected as the wheel forces increased with increased velocity. Furthermore, the relative displacement obtained in all openings when driving at 50 km/h is linearly scaled in y-direction which was obvious from using a visual best fit factor. It was observed that a velocity increase in physical test results in a similar increase of the relative displacement as in simulation.

The last studied parameter is the damping. The physical test data is compared with two simulation cases with two modal damping values. A minimum and maximum model damping value of 2% respectively 15% was chosen. For instance, simulation with 15% modal damping is over-predicting the relative displacement found in physical test. The specific modes which gave over-prediction or under-prediction compared to physical test may be identified using a bandpass filter. Bandpass filter analysis may result in better understanding of the simulation model, and thus how it can be improved. In general when comparing simulation and physical test data for all openings and all load cases it could be concluded that a 15% damping generally slightly under-predicts physical test results, whereas a 2% damping value generally gives an over-prediction.

Using the existing model the relative displacement predictions are not reliable. The model needs to be improved. But, it was concluded that the simulation procedure can be used to predict in relative terms the opening displacement in the respect that it predicts increasing or decreasing displacement due to a structural change sufficiently well.

5.2 Future work

The accelerometers used during the physical test phase are not accurate at frequencies below 4 Hz. The accelerometer output is converted to displacement data. This converting tool may contribute to calculation errors especially at low frequencies. Thus, a displacement measuring equipment which can capture displacement at frequencies as low as 1 Hz is desired in order increase the accuracy of a displacement correlation study.

Furthermore, the modal damping model implemented into the body rig simulation gave inconclusive results. Thus, a profound study of the modal damping may result in improved correlation between physical test and simulation data. The deviation between simulation and physical test is likely caused by incorrect simulation modes. It is essential to identify deficient modes and understand why these modes give under-predictions or over-predictions when compared with results of physical test.

To get a better picture of the RBM a further Adams study was performed. This obtained by linearization around the operational state in which only gravity act. The modes occurring in physical test are also affected by varying track load. One possibility solution could be to linearize the car around an operational state in the model were respect is taken also to the forces obtained from the roads.

Furthermore, the physical test contains both RBM and structural modes at frequencies below 20 Hz. These RBM are excluded by simply applying a cutoff frequency at 20 Hz. The structural modes needs to be separated from rigid body motions in order to enable a correlation study between simulation and physical test at frequencies below 20 Hz.

Bibliography

[1] Scharff, Robert; Mullen, Keith; Corinchock, John A. (1990). *Complete automotive estimating.* Delmar Publishers. p. 172. ISBN 9780827335851.

[2] Jacobsson, C. and Jörud, A. "Improving a Complete Vehicle Model for Solidity Simulations" Master's thesis, Lunds Tekniska Högskola, Department of Mechanics 2018. [Online]. Available: `http://lup.lub.lu.se/student-papers/record/8949419`, Accessed: May 05, 2019

[3] *"A Brief Introduction to Piezoelectric Sensor Switch And its Working Procedure."* [Online]. Available: `https://www.edgefx.in/piezoelectric-sensor-switch-working/`, Accessed: May 05, 2019

[4] "Piezoelectric Sensor". [Online]. Available: `https://www.sciencedirect.com/topics/engineering/piezoelectric-sensor`, Accessed: May 06, 2019

[5] *RoaDyn® S660 - Wheel Force Transducer for Racing, SUVs, Transportersand Light Trucks.* Kistler Group. [Online]. Available: `https://www.kistler.com/?type=669&fid=88438&model=document&callee=frontend`, Accessed: May 07, 2019

[6] *Force transducers based on strain gauges.* Sweden: HBM [Online]. Available: `https://www.hbm.com/en/6697/how-does-a-force-transducer-actually-work/`, Accessed: May 07, 2019

[7] *Adams: The Multibody Dynamics Simulation Solution,* MSC software. [Online]. Available: `https://www.mscsoftware.com/product/adams`, Accessed: May 10, 2019

[8] *Ansa,* BETA CAE Systems. [Online]. Available: `https://www.beta-cae.com/Ansa.htm`, Accessed: May 10, 2019

[9] *Meta,* BETA CAE Systems. [Online]. Available: `https://www.beta-cae.com/meta.htm`, Accessed: May 10, 2019

[10] *MSC Nastran 2012.* Dynamic Analysis, Users Guide. [Online]. Available: https://www.mscsoftware.com, Accessed: May 11, 2019

[11] Hällered Proving Grounds. *Hällered Proving Ground - Facilities & Safety Regulations*. Volvo Car Corporation, 2018.

[12] *Siemens LMS. LMS FAQ 630 - Integration,* Siemens AG, 2016.

[13] "Rotations and Orientation." [Online]. Available: https://www.cs.utexas.edu/~theshark/courses/cs354/lectures/cs354-14.pdf., Accessed: May 18, 2019

[14] "Difference Between RMS and Average." [Online]. Available: http://www.differencebetween.net/science/difference-between-rms-and-average/, Accessed: May 20, 2019

[15] Steven W. Smith, Ph.D. "The Scientist and Engineer's Guide to Digital Signal Processing - The Fast Fourier Transform." [Online]. Available: https://www.dspguide.com/ch12/2.htm, Accessed: May 20, 2019

[16] Siemens. "The Gibbs Phenomenon". [Online]. Available: https://community.plm.automation.siemens.com/t5/Testing-Knowledge-Base/The-Gibbs-Phenomenon/ta-p/481867, Accessed on: May 17, 2019.

A

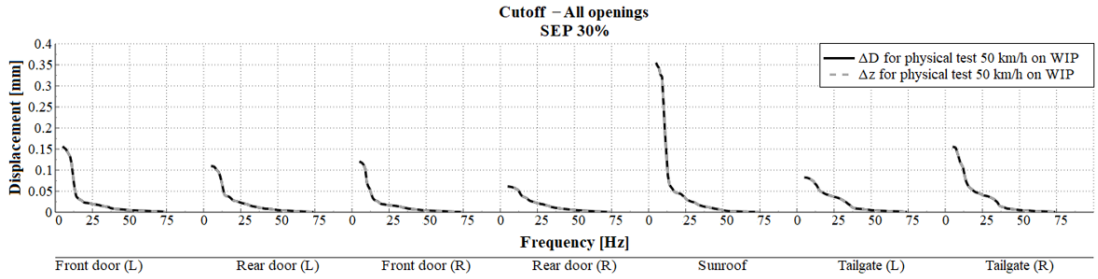

Figure A.1: Cut-off filter applied on all closure openings of the car with SEP 30% value for ΔD and Δz. Physical test speed 50 km/h with $\xi = 2\%$ driving on WIP.

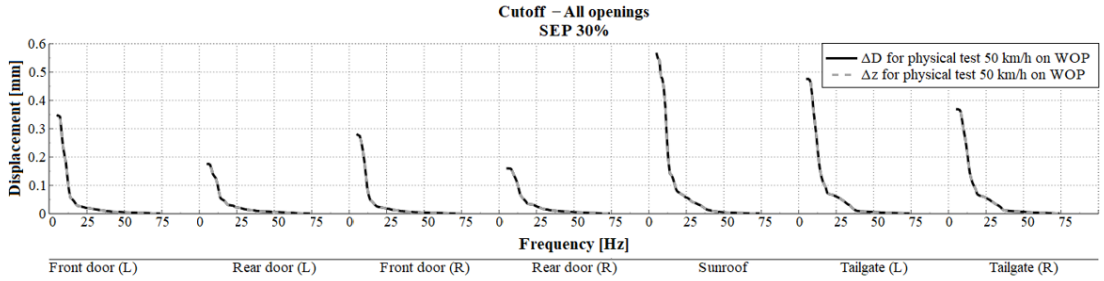

Figure A.2: Cut-off filter applied on all closure openings of the car with SEP 30% value for ΔD and Δz. Physical test speed 50 km/h with $\xi = 2\%$ driving on WOP.

B

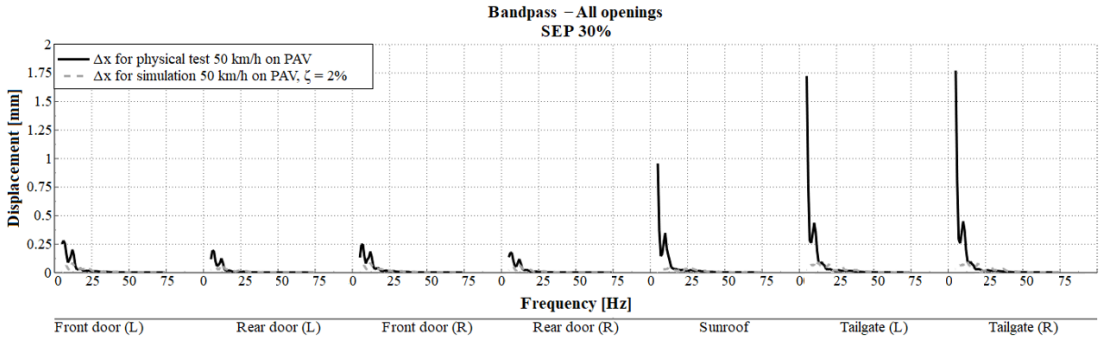

Figure B.1: Bandpass filter applied on all closure openings of the car with SEP 30% value for Δx. Physical test speed 50 km/h and simulation speed 50 km/h with $\xi = 2\%$ driving on PAV.

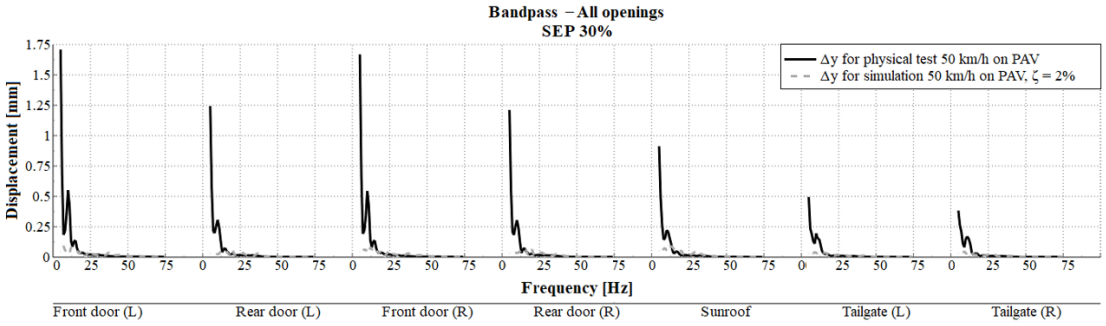

Figure B.2: Bandpass filter applied on all closure openings of the car with SEP 30% value for Δy. Physical test speed 50 km/h and simulation speed 50 km/h with $\xi = 2\%$ driving on PAV.

C

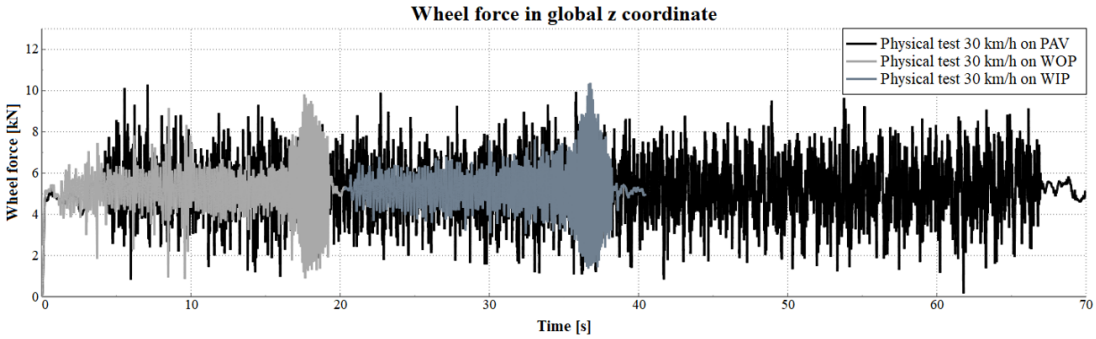

Figure C.1: Wheel force in global Z for physical test speed 30 km/h driving on PAV, WOP and WIP

D

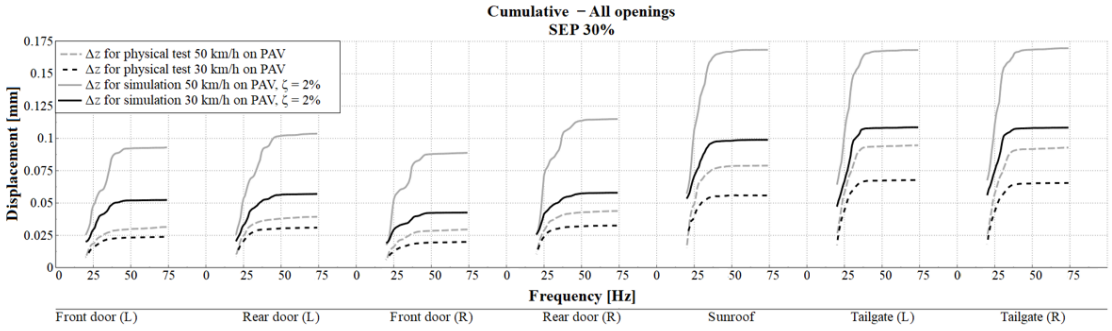

Figure D.1: Cumulative filter applied on all closure openings of the car with SEP 30% value for Δz. Physical test speed 50 km/h, physical test speed 30 km/h, simulation speed 50 km/h with $\xi = 2\%$ and simulation speed 30 km/h with $\xi = 2\%$ driving on PAV.

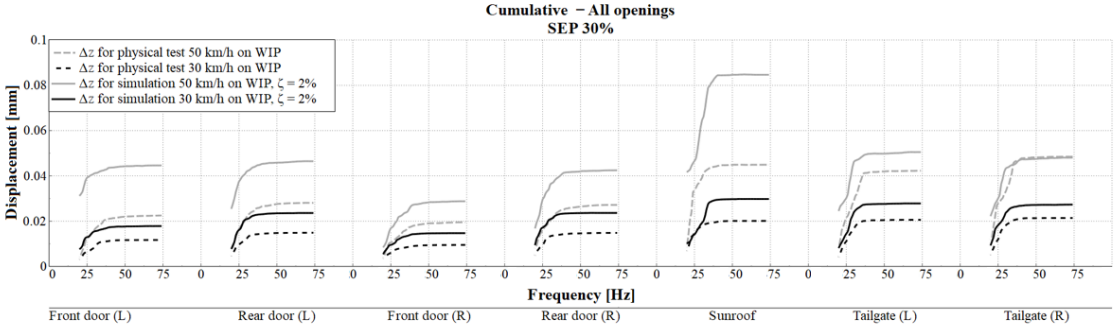

Figure D.2: Cumulative filter applied on all closure openings of the car with SEP 30% value for Δz. Physical test speed 50 km/h, physical test speed 30 km/h, simulation speed 50 km/h with $\xi = 2\%$ and simulation speed 30 km/h with $\xi = 2\%$ driving on WIP.

E

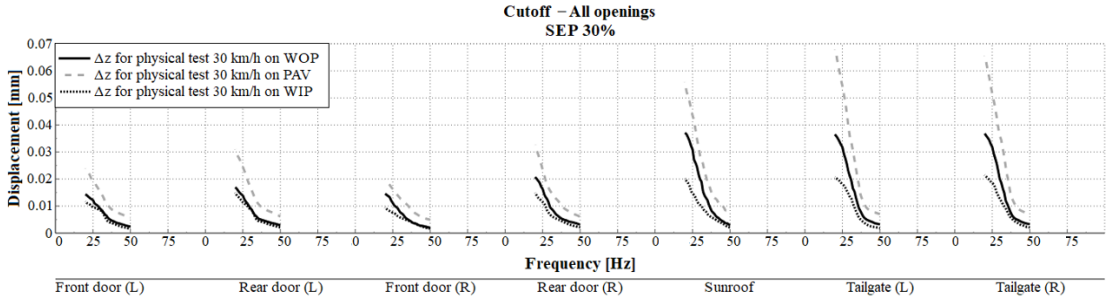

Figure E.1: Cut-off filter applied on all closure openings of the car with SEP 30% value for Δz. Physical test speed 30 km/h driving on WOP, PAV and WIP.

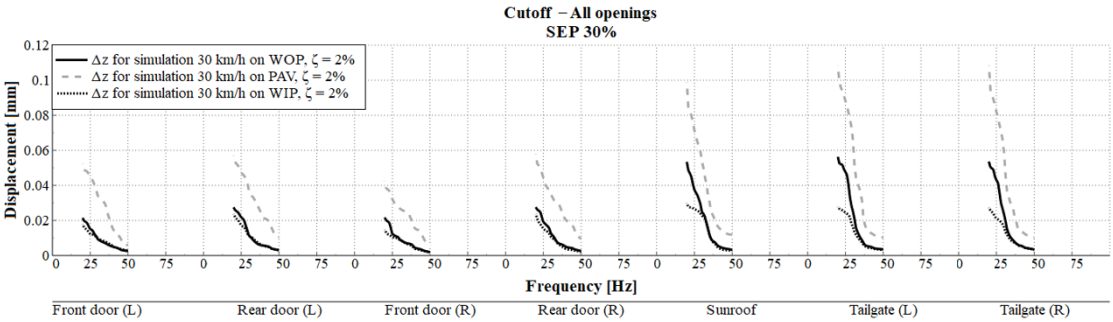

Figure E.2: Cut-off filter applied on all closure openings of the car with SEP 30% value for Δz. Simulation speed 30 km/h with $\xi = 2\%$ driving on WOP, PAV and WIP.

F

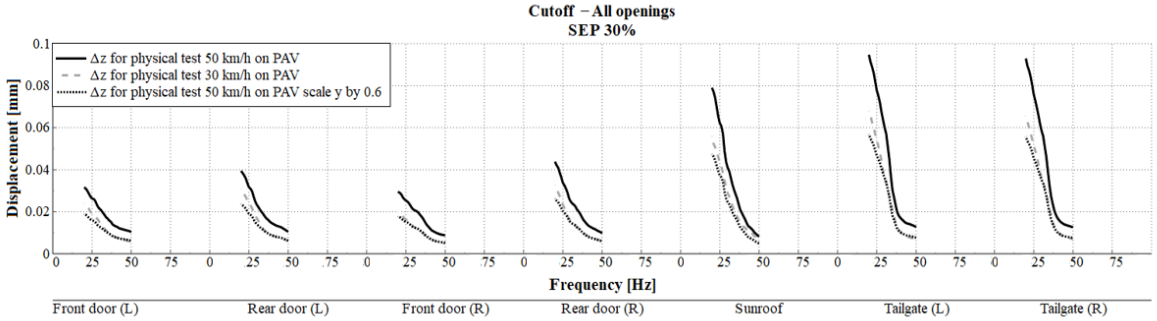

Figure F.1: Cut-off filter applied on all closure openings of the car with SEP 30% value for Δz. Physical test speed 50 km/h and physical test speed 30 km/h driving on PAV. The physical test speed 50 km/h is scaled in vertical direction by factor 0.6.

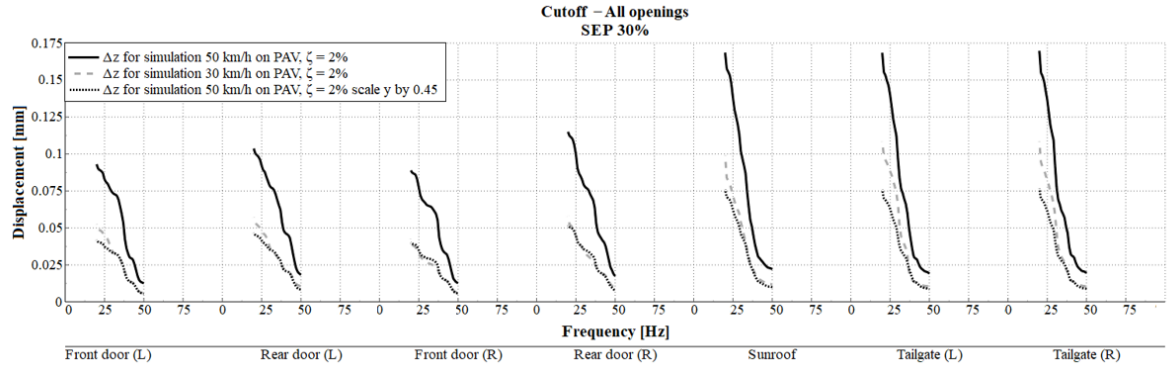

Figure F.2: Cut-off filter applied on all closure openings of the car with SEP 30% value for Δz. Simulation speed 50 km/h with $\xi = 2\%$ and simulation speed 30 km/h with $\xi = 2\%$ driving on PAV. The physical test speed 50 km/h is scaled in vertical direction by factor 0.60.

G

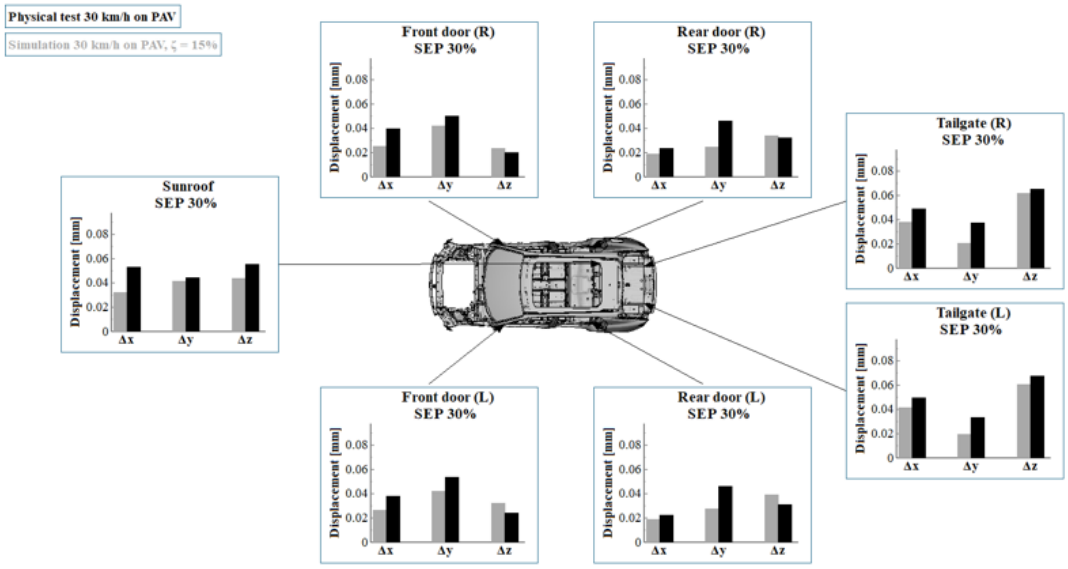

Figure G.1: Mean value applied on all closure openings of the car with SEP 30% value for Δx, Δy and Δz. Physical test speed 30 km/h and simulation speed 30 km/h with $\xi = 15\%$ driving on PAV.

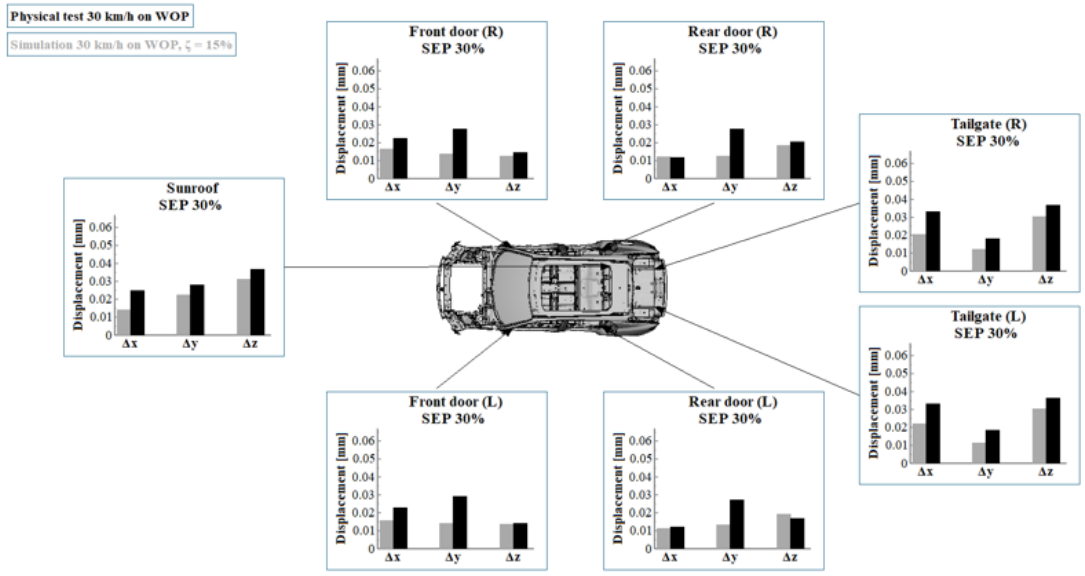

Figure G.2: Mean value applied on all closure openings of the car with SEP 30% value for Δx, Δy and Δz. Physical test speed 30 km/h and simulation speed 30 km/h with $\xi = 15\%$ driving on WOP.

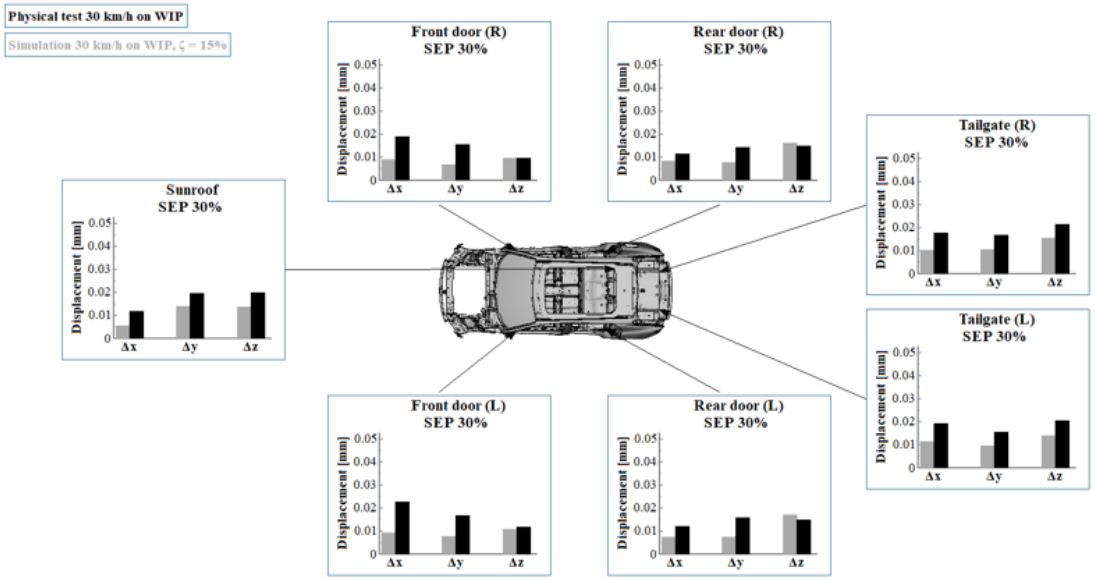

Figure G.3: Mean value applied on all closure openings of the car with SEP 30% value for Δx, Δy and Δz. Physical test speed 30 km/h and simulation speed 30 km/h with $\xi = 15\%$ driving on WIP.